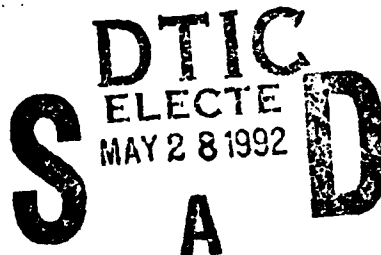




**STRESS AND RELIABILITY ANALYSIS OF LAYERED  
COMPOSITE CYLINDERS UNDER THERMAL SHOCK:**

**VOLUME 3.**

R.A. Heller  
S. Thangjitham  
X. Wang



Department of Engineering Science and Mechanics  
Virginia Polytechnic Institute and State University  
Blacksburg VA 24061-0219

April 1992

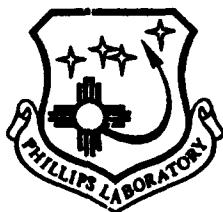
Final Report

APPROVED FOR PUBLIC RELEASE; DISTRIBUTION UNLIMITED

92-13881



92 5 28 096



**PHILLIPS LABORATORY**  
**Propulsion Directorate**  
**AIR FORCE SYSTEMS COMMAND**  
**EDWARDS AIR FORCE BASE CA 93523-5000**

## NOTICE

When U.S. Government drawings, specifications, or other data are used for any purpose other than a definitely related Government procurement operation, the fact that the Government may have formulated, furnished, or in any way supplied the said drawings, specifications, or other data, is not to be regarded by implication or otherwise, or in any way licensing the holder or any other person or corporation, or conveying any rights or permission to manufacture, use or sell any patented invention that may be related thereto.

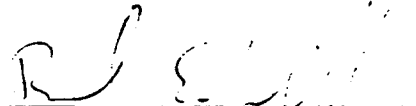
## FOREWORD

This Final 3 Volume Report was prepared by the Department of Engineering Science and Mechanics, Virginia Polytechnic Institute and State University, Blacksburg VA, under contact F04611-87-K-0010 for Operating Location AC, Phillips Laboratory (AFSC), Edwards AFB CA 93523-5000. OLAC PL Project Manager was Chi T. Liu.

This report has been reviewed and is approved for release and distribution in accordance with the distribution statement on the cover and on the SF Form 298.



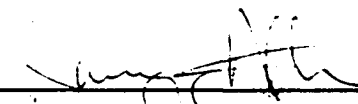
CHI T. LIU  
Project Manager



BERNARD E. WILKERSON, CAPT, USAF  
Chief, Propellants Branch



WAYNE L. PRITZ  
Director,  
Components Engineering Division



RANNEY G. ADAMS  
Public Affairs Director

REPORT DOCUMENTATION PAGE			Form Approved OMB No. 0704-0188	
<small>Public reporting burden for this collection of information is estimated to average 1 hour per response, including the time for reviewing instructions, searching existing data sources, gathering and maintaining the data needed, and completing and reviewing the collection of information. Send comments regarding this burden estimate or any other aspect of this collection of information, including suggestions for reducing this burden, to Washington Headquarters Services, Directorate for Information Operations and Reports, 1215 Jefferson Davis Highway, Suite 1204, Arlington, VA 22202-4302, and to the Office of Management and Budget, Paperwork Reduction Project (0704-0188), Washington, DC 20503.</small>				
1. AGENCY USE ONLY (Leave blank)		2. REPORT DATE April 1992		3. REPORT TYPE AND DATES COVERED Technical Report 87-9/91
4. TITLE AND SUBTITLE Stress and Reliability Analysis of Layered Composite Cylinders under Thermal Shock			5. FUNDING NUMBERS F04611-87-K-0010/P0001	
6. AUTHOR(S) Heller, R. A., Thangjitham, S., and Wang, X.			PR: 3059 TA: 004G	
7. PERFORMING ORGANIZATION NAME(S) AND ADDRESS(ES) Department of Engineering Science and Mechanics Virginia Polytechnic Institute and State University Blacksburg, VA 24061-0219			8. PERFORMING ORGANIZATION REPORT NUMBER	
9. SPONSORING/MONITORING AGENCY NAME(S) AND ADDRESS(ES) Department of the Air Force OLAC, Phillips Lab (AFSC) Edwards AFB, CA 90523-5000 Dr. C. T. Liu, OLAC/PL/RCP			10. SPONSORING/MONITORING AGENCY REPORT NUMBER PL-TR-91-3068 V3	
11. SUPPLEMENTARY NOTES  This is the third part of a three part final report. COSATI Codes: 07/02: 20/11				
12a. DISTRIBUTION/AVAILABILITY STATEMENT  Public Release; Distribution Unlimited			12b. DISTRIBUTION CODE	
13. ABSTRACT (Maximum 200 words) The state of stress in a cylindrical structure consisting of multiple layers of carbon-carbon composite and subjected to thermal and pressure shock are analyzed using an elasticity approach. The reliability of the structure based on the weakest link concept and the Weibull distribution is also calculated. Coupled thermo-elasticity is first assumed and is shown to be unnecessary for the material considered. The effects of external and internal thermal shock as well as a superimposed pressure shock are examined. It is shown that for the geometry chosen the structure may fail when exposed to thermal shock alone while a superimposed pressure shock can mitigate the probability of failure.				
14. SUBJECT TERMS Carbon-carbon, thermal shock, pressure shock, coupled thermo-elasticity, composite cylinder, reliability, probability of failure, weakest link, Weibull distribution.			15. NUMBER OF PAGES 72	
			16. PRICE CODE	
17. SECURITY CLASSIFICATION OF REPORT Unclassified	18. SECURITY CLASSIFICATION OF THIS PAGE Unclassified	19. SECURITY CLASSIFICATION OF ABSTRACT Unclassified	20. LIMITATION OF ABSTRACT SAR	

Accession For	
NTIS CRA&I	<input checked="" type="checkbox"/>
DTIC TAB	<input type="checkbox"/>
Unannounced	<input type="checkbox"/>
Justification	
By	
Distribution/	
A-1	

## Table of Contents

List of Illustrations .....	iv
List of Tables .....	v
SECTION 1. INTRODUCTION .....	1
SECTION 2. COUPLED THERMAL SHOCK PROBLEM .....	3
Governing Equations .....	3
Method of Complex Frequency Response Functions .....	4
Boundary Conditions .....	5
Reliability Analysis .....	8
Illustrative Examples .....	9
SECTION 3. ORTHOTROPIC CYLINDER PROBLEM .....	23
Temperature Analysis .....	23
Stress Analysis .....	24
Reliability Analysis .....	28
Illustrative Examples .....	30

<b>SECTION 4. CONCLUSIONS</b>	<b>59</b>
-------------------------------	-----------

<b>REFERENCES</b>	<b>60</b>
-------------------	-----------

## List of Illustrations

Figure 1. Configuration of the Cylinder. ....	7
Figure 2. Input Temperature (K). ....	12
Figure 3. Tangential Stress on the Innermost Surface under Internal Thermal Shock. .	13
Figure 4. Tangential Stress on the Outermost Surface under Internal Thermal Shock. .	14
Figure 5. Probability of Failure of the Cylinder, Innermost and Outermost Layer, under Internal Thermal Shock. ....	15
Figure 6. Probability of Failure of the Cylinder, for Different Coupling Coefficients, under Internal Thermal Shock. ....	16
Figure 7. Tangential Stress on the Innermost Surface under External Thermal Shock. .	18
Figure 8. Tangential Stress on the Outermost Surface under External Thermal Shock. .	19
Figure 9. Probability of Failure of the Cylinder, Innermost and Outermost Layer, under External Thermal Shock. ....	20
Figure 10. Probability of Failure of the Cylinder, for Different Coupling Coefficients, under External Thermal Shock. ....	21
Figure 11. Configuration of the Cylinder. ....	31
Figure 12. Tangential Stress in Parameter Study (Case 1). ....	33
Figure 13. Tangential Stress in Parameter Study (Case 2). ....	34
Figure 14. Tangential Stress in Parameter Study (Case 3). ....	35
Figure 15. Tangential Stress in Parameter Study (Case 4). ....	36
Figure 16. Reliability of the Cylinder in Parameter Study (Case 4). ....	37
Figure 17. Probability of Failure of Fiber Layers through the Thickness under Combined Thermal and Pressure Loading. ....	39
Figure 18. Probability of Failure of the Cylinder under Combined Thermal and Pressure Loading. ....	40

Figure 19.	Tangential Stresses on the Innermost Surface (Matrix Layer); Thermal and Pressure Loading. ....	41
Figure 20.	Tangential Stresses on the Inner Surface of Layer 2 (Fiber Layer); Thermal and Pressure Loading. ....	42
Figure 21.	Tangential Stresses on the Outer Surface of Layer 32 (Fiber Layer); Thermal and Pressure Loading. ....	43
Figure 22.	Tangential Stresses on the Outermost Surface (Matrix Layer); Thermal and Pressure Loading. ....	44
Figure 23.	Tangential Stresses on the Innermost Surface (Matrix Layer) Subjected to Internal Thermal Shock and Internal Pressure. ....	45
Figure 24.	Tangential Stresses on the Inner Surface of Layer 2 (Fiber Layer) Subjected to Internal Thermal Shock and Internal Pressure. ....	46
Figure 25.	Tangential Stresses on the Outer Surface of Layer 32 (Fiber Layer) Subjected to Internal Thermal Shock and Internal Pressure. ....	47
Figure 26.	Tangential Stresses on the Outermost Surface (Matrix Layer) Subjected to Internal Thermal Shock and Internal Pressure. ....	48
Figure 27.	Tangential Stresses in Different Matrix Layers Subjected to Internal Thermal Shock. ....	49
Figure 28.	Tangential Stresses in Different Fiber Layers Subjected to Internal Thermal Shock. ....	50
Figure 29.	Maximum Tangential Stresses in Matrix Layers through the Thickness of the Cylinder. ....	51
Figure 30.	Maximum Tangential Stresses in Fiber Layers through the Thickness of the Cylinder. ....	52
Figure 31.	Maximum Probability of Failure of Fiber Layers through the Thickness of the Cylinder. ....	53
Figure 32.	Maximum Probability of Failure of Fiber Layers through the Thickness of the Cylinder for Different Rise Times. ....	54
Figure 33.	Reliability of the Matrix Layers Subjected to Thermal Shock and Internal Pressure with Different Amplitudes. ....	56
Figure 34.	Reliability of the Fiber Layers Subjected to Thermal Shock and Internal Pressure with Different Amplitudes. ....	57
Figure 35.	Reliability of the Cylinder Subjected to Thermal Shock and Internal Pressure with Different Amplitudes. ....	58

## List of Tables

Table 1. Geometric, Thermal and Mechanical Parameters for Isotropic Materials. . . . .	11
Table 2. Coupling Coefficients of Some Engineering Materials . . . . .	22
Table 3. Geometric, Thermal and Mechanical Parameters for Carbon-Carbon. . . . .	32



## SECTION 1. INTRODUCTION

Carbon-carbon composite with its superior mechanical properties at elevated temperatures is utilized in structures subjected to high temperatures and severe thermal gradients such as rocket nozzles and reentry space vehicles. Though the material retains most of its strength and stiffness when heated, it is brittle and as all composites is afflicted by statistically distributed imperfections: matrix poor regions, broken fibers and voids. Such imperfections are more prevalent in large components than in small, laboratory specimens hence structural reliability analysis must account for a probability based size effect.

In Part I [1] of this report, experimental results on mechanical properties and on size effect in carbon-carbon have been presented while Part II [2] reports the development of a structural reliability analysis based on the "weakest link" principle. The present, Part III, applies the data and the reliability analysis to a cylindrical structure of this material subjected to thermal shock combined with internal pressure.

Sudden changes in temperature may produce severe thermal stresses in these structures. In such situations, the velocity of the strain induced by temperature should be considered. For some materials, the effect of thermo-mechanical coupling is important when subjected to a thermal shock. Earlier studies on coupled thermoelasticity can be found in references [3-5]. It is observed that when temperature changes at a very high rate, the effect of volume change cannot be neglected. A coupling term, defined as the contribution of energy resulting from the volume change, is to be added to the classical Fourier heat conduction equation [3]. As a result, in addition to the temperature function, there is also the volume strain function in the corrected relation. Under this circumstance, the temperature distribution in the structure cannot be independently obtained by considering only the heat conduction problem. The coupled heat conduction equation and the equilibrium equation must be solved simultaneously.

A coupled thermal stress problem of an infinite axisymmetric solid cylinder is analyzed by Takeuti and Tanigawa [6,7]. To obtain the solution, a harmonic function is introduced to constitute the relation between the volume strain and temperature functions. The technique of Laplace transform is used in these papers.

The complex frequency response functions for temperatures, displacements, and stresses for the general uncoupled thermoelasticity problem in a long multilayered cylinder can be found in Thangjiitham, Heller, and Singh [8]. The applications of these functions to stress analysis under steady harmonic thermal loadings are found in references [9,10].

In 1978, Kalam and Tauchert [11] obtained the solution of stresses in a hollow orthotropic single layer cylinder subjected to an asymmetric steady-state plane temperature distribution by the method of Airy's stress functions in Fourier series form. In 1986, Hyer and Cooper [12] analyzed stresses and deformations in single layer and multiple layer cross-ply composite cylinders due to a circumferential temperature gradient by an elastic approach. In that paper, the temperature does not vary along the axis and the radius of the cylinders, but is in the form of  $\Delta T_0 + \Delta T_1 \cos \theta$ .

Parida and Das [13] investigated the transient plane thermal stresses in a thin circular disc of orthotropic material due to an instantaneous point heat source. The method of separation of variables was applied in solving the heat conduction equation for temperature distribution, and the stress function was applied in the stress and strain analysis.

In recent years, more work was reported on transient thermal stresses in composite material structures. In 1989, Tauchert [14] studied the effects of thermal shock on simply supported, thin orthotropic rectangular plates. The displacements contain the quasistatic part which is an exact Levy-type solution and the dynamic part which was obtained by Galerkin's method and Laplace transformation. Tanigawa, Murakami and Ootao [15] analyzed on transient thermal stresses in a laminated composite beam made of different materials in multilayers. The temperature of the beam was assumed to vary in the direction of the thickness, and the heat conduction equation was solved by Laplace transform. The thermal stresses were obtained by elementary beam theory and Airy's thermal stress functions. Wang and Chou [16] worked on transient interlaminar thermal stresses in symmetric angle ply composite laminates with infinite length and finite width. The temperature varies in the width direction. The heat conduction equation was solved by the separation of variables method and the equilibrium equation was analyzed by zeroth-order perturbation technique.

In Section 2 of this report, thermal stresses in a long hollow multilayered cylinder subjected to sudden axisymmetric external and internal temperature are analyzed. Coupling resulting from the mutual influence of material thermal and mechanical parameters will be examined while the inertial effect will be neglected. The method of complex frequency response functions together with the Fourier transform technique is utilized here. Due to the linear nature of the problem, the time response functions for temperatures, displacements, and stresses are obtained by applying inverse Fourier transforms to the product of the complex frequency response functions and the Fourier transform of the input temperature. The integral of the inverse Fourier transform in this problem is found to involve only those of real functions. As a result, standard numerical techniques can be implemented in the inversion procedure. The reliability of the cylinder is analyzed based on the "weakest link" principle and the two parameter Weibull distribution.

For carbon-carbon composite, the coupling parameters are very small, and the coupling effect can be neglected. In Section 3 of this report, uncoupled thermal stresses and reliability are investigated in a long hollow layered orthotropic cylinder subjected to asymmetric thermal shock and internal pressure. The method of Laplace transform and Fourier series with the elasticity approach are applied in this problem. The "weakest link" principle which takes into consideration both the applied stresses and the effected volume of material is used again in the reliability analysis, but a three parameter Weibull distribution is applied.

## SECTION 2. COUPLED THERMAL SHOCK PROBLEM

### Governing Equations

The heat conduction equation for a plane axisymmetric coupled thermoelasticity problem expressed in terms of cylindrical coordinates is given as [17-19]

$$\nabla^2 T = \frac{1}{\gamma} \frac{\partial T}{\partial t} + \frac{\alpha^2 E T_R}{\gamma \rho c_v (1 - 2\nu)} \frac{\partial e}{\partial t} \quad (1)$$

where  $T(r,t)$  and  $e(r,t)$  are the temperature and volume strain functions,  $r$  and  $t$  are the radial coordinate and time,  $\nabla^2$  is the Laplacian operator,  $E$  and  $\nu$  are the modulus of elasticity and Poisson's ratio, and  $\alpha$ ,  $\gamma$ ,  $\rho$ , and  $c_v$  are the coefficients of thermal expansion and of thermal diffusivity, mass density, and specific heat, respectively.

The thermo-mechanical coupling parameter,  $\delta$ , is expressed in terms of the material mechanical and thermal properties as [17-19]

$$\delta = \frac{1 + \nu}{1 - \nu} \frac{\alpha^2 E T_R}{(1 - 2\nu) \rho c_v} \quad (2)$$

where  $T_R$  is the reference temperature.

In terms of the thermo-mechanical coupling parameter,  $\delta$ , Eq. 1 can be rewritten as

$$\nabla^2 T = \frac{1}{\gamma} \frac{\partial T}{\partial t} + \frac{\delta}{\gamma \alpha} \frac{1 - \nu}{1 + \nu} \frac{\partial e}{\partial t} \quad (3)$$

where the second term on the right-hand side of the above equation represents the coupling effect of volume strain to the temperature field.

The equation of equilibrium for the case of plane strain under axisymmetric heating is given, in terms of cylindrical coordinates, as [18]

$$\frac{\partial e}{\partial r} = \frac{1 + \nu}{1 - \nu} \alpha \frac{\partial T}{\partial r} \quad (4)$$

The volume strain function,  $e$ , and radial displacement,  $u(r,t)$ , are connected through the relationship

$$e = \frac{\partial u}{\partial r} + \frac{u}{r} \quad (5)$$

In terms of the volume strain, radial displacement, and temperature, the nontrivial stress components are obtained as [18]

$$\sigma_r = \frac{\nu E}{(1 + \nu)(1 - 2\nu)} e + \frac{E}{1 + \nu} \frac{\partial u}{\partial r} - \frac{\alpha E}{1 - 2\nu} T \quad (6)$$

$$\sigma_\theta = \frac{\nu E}{(1+\nu)(1-2\nu)} e + \frac{E}{1+\nu} \frac{u}{r} - \frac{\alpha E}{1-2\nu} T \quad (7)$$

where  $\sigma_r(r,t)$  and  $\sigma_\theta(r,t)$  are the radial and tangential stress components, respectively.

The variables in Eqs. 3 through 7 are written in terms of dimensionless variables with the following transformations:

$$\begin{aligned} r &\rightarrow \frac{r}{r_R}, & \nabla^2 &\rightarrow r_R^2 \nabla^2, & t &\rightarrow \frac{\gamma_R t}{r_R^2} \\ T &\rightarrow \frac{T}{T_R}, & e &\rightarrow \frac{e}{\alpha_R T_R}, & \sigma_r &\rightarrow \frac{\sigma_r}{\alpha_R T_R E_R}, & \sigma_\theta &\rightarrow \frac{\sigma_\theta}{\alpha_R T_R E_R} \\ E &\rightarrow \frac{E}{E_R}, & \gamma &\rightarrow \frac{\gamma}{\gamma_R}, & \alpha &\rightarrow \frac{\alpha}{\alpha_R} \end{aligned} \quad (8)$$

where  $r_R$ ,  $E_R$ ,  $\alpha_R$ , and  $\gamma_R$  are the characteristic radius, reference modulus of elasticity, and reference coefficients of thermal expansion and of thermal diffusivity, respectively.

Integrating Eq. 4, the volume strain function is obtained as

$$e = \frac{1+\nu}{1-\nu} \alpha (T + \Phi) \quad (9)$$

where  $\Phi(t)$  is an unknown function of time.

Substituting Eq. 9 into Eq. 3, the coupled heat conduction equation becomes

$$\nabla^2 T = \frac{1+\delta}{\gamma} \frac{\partial T}{\partial t} + \frac{\delta}{\gamma} \frac{\partial \Phi}{\partial t} \quad (10)$$

where the heat conduction equation is now decoupled. The coupling effect is represented by the coupling parameter,  $\delta$ , and the unknown function of time,  $\Phi$ . Because the volume strain function does not appear in the heat conduction equation, the equation involves only the temperature and  $\Phi$  function.

## Method of Complex Frequency Response Functions

When a sinusoidal temperature input of some amplitude and frequency,  $\omega$ , is applied to the structure, the responses, such as temperatures, strains, displacements and stresses in the structure, will become sinusoidal with the same frequency as the input but will have different amplitudes and will undergo phase shifts [8-10,18,19]. To analyze the problem under this type of temperature input, the method of complex frequency response functions is expedient. The complex frequency response function is defined as the output response resulting from a sinusoidal temperature input of unit amplitude and frequency,  $\omega$ . To utilize the method of complex frequency response functions, the following solutions are assumed.

$$e = \tilde{e} \exp(i\omega t), \quad T = \tilde{T} \exp(i\omega t), \quad \Phi = \tilde{\Phi} \exp(i\omega t) \quad (11 \text{ a, b, c})$$

$$u = \tilde{u} \exp(i\omega t), \quad \sigma_r = \tilde{\sigma}_r \exp(i\omega t), \quad \sigma_\theta = \tilde{\sigma}_\theta \exp(i\omega t) \quad (11 \text{ d, e, f})$$

where  $\tilde{e}(r, \omega)$ ,  $\tilde{T}(r, \omega)$ ,  $\tilde{\Phi}(\omega)$ ,  $\tilde{u}(r, \omega)$ ,  $\tilde{\sigma}_r(r, \omega)$ , and  $\tilde{\sigma}_\theta(r, \omega)$  are the corresponding complex frequency response functions for  $e$ ,  $T$ ,  $\Phi$ ,  $u$ ,  $\sigma_r$ , and  $\sigma_\theta$ , respectively, and  $i = \sqrt{-1}$ .

Substituting Eqs. 11(b) and 11(c) into Eq. 10, the coupled heat conduction equation, expressed in terms of the complex frequency response functions,  $\tilde{T}$  and  $\tilde{\Phi}$  is given as

$$\nabla^2 \tilde{T} = \frac{(1+\delta)}{\gamma} i\omega \tilde{T} + \frac{\delta}{\gamma} i\omega \tilde{\Phi} \quad (12)$$

where the above equation is a complex differential equation with  $\omega$  as a parameter.

The general solution of Eq. 12 is obtained as

$$\tilde{T} = C_1 Br(ar) + C_2 Kr(ar) - \frac{\delta}{1+\delta} \tilde{\Phi} \quad (13)$$

where  $C_k(\omega)$ ,  $k=1,2$ , are the complex constants of integration to be evaluated by applying the appropriate boundary conditions,  $a(\omega) = \sqrt{(1+\delta)\omega/\gamma}$ , and  $Br(x)$  and  $Kr(x)$  are defined as

$$Br(x) = ber(x) + ibei(x), \quad Kr(x) = ker(x) + ikei(x) \quad (14)$$

where  $ber(x)$ ,  $bei(x)$ ,  $ker(x)$ , and  $kei(x)$  are the Kelvin functions of order zero [20].

Substituting Eq. 13 into 9 and in conjunction with Eqs. 11(a), (b), and (c), the frequency response function for the volume strain,  $\tilde{e}$ , is given as

$$\tilde{e} = \frac{(1+\nu)}{(1-\nu)} \alpha \left[ C_1 Br(ar) + C_2 Kr(ar) + \frac{1}{1+\delta} \tilde{\Phi} \right] \quad (15)$$

Upon substituting the above expression into Eq. 5, the complex frequency response function for displacement,  $\tilde{u}$ , is obtained by direct integration as

$$\tilde{u} = \frac{1+\nu}{1-\nu} \alpha \left[ C_1 r^{-1} \int^r \xi Br(a\xi) d\xi + C_2 r^{-1} \int^r \xi Kr(a\xi) d\xi \right] + C_3 r^{-1} + \frac{(1+\nu)\alpha}{2(1-\nu)(1+\delta)} r \tilde{\Phi} \quad (16)$$

Similarly, upon substituting  $\tilde{T}$  in Eq. 13,  $\tilde{e}$  in Eq. 15 and  $\tilde{u}$  in Eq. 16 into Eqs. 6 and 7, the complex frequency response functions for stress components  $\tilde{\sigma}_r$  and  $\tilde{\sigma}_\theta$  are obtained as

$$\begin{aligned} \tilde{\sigma}_r = & -\frac{\alpha E}{1-\nu} \left[ C_1 r^{-2} \int^r \xi Br(a\xi) d\xi + C_2 r^{-2} \int^r \xi Kr(a\xi) d\xi \right] - \frac{E}{1+\nu} C_3 r^{-2} \\ & + \frac{\alpha E [1 + 2\delta(1-\nu)]}{2(1-\nu)(1-2\nu)(1+\delta)} \tilde{\Phi} \end{aligned} \quad (17)$$

$$\begin{aligned} \tilde{\sigma}_\theta = & \frac{\alpha E}{1-\nu} C_1 \left[ r^{-2} \int^r \xi Br(a\xi) d\xi - Br(ar) \right] + \frac{\alpha E}{1-\nu} C_2 \left[ r^{-2} \int^r \xi Kr(a\xi) d\xi - Kr(ar) \right] \\ & + \frac{E}{1+\nu} C_3 r^{-2} + \frac{\alpha E [1 + 2\delta(1-\nu)]}{2(1-\nu)(1-2\nu)(1+\delta)} \tilde{\Phi} \end{aligned} \quad (18)$$

where  $C_k$ ,  $k=1,2,3$ , are the integration constants.

## Boundary Conditions

For each layer of a multilayered cylinder, there are a total of four unknown constants, namely,  $C_1$ ,  $C_2$ ,  $C_3$ , and  $\tilde{\Phi}$ , to be simultaneously evaluated by a set of proper boundary conditions. Consequently, for a  $J$ -layered cylinder, there are  $4J$  unknown constants to be evaluated. This is accomplished by applying the temperature, heat flux, displacement, and traction boundary conditions at the bounding surfaces and at the interfaces of any two adjacent layers.

In this study, a hollow  $J$ -layer cylinder (Fig. 1) is considered. Because there exist no induced stresses in the air core (layer 1), only uncoupled temperature analysis is required for this layer. The remaining  $(J-1)$  layers are stressed layers for which the solutions of coupled thermoelasticity are sought. Depending on the location of the applied input temperature, there

are two boundary value problems to be considered, i.e., the input temperature is uniformly applied (a) on the outer surface of the outermost ( $J$ th) layer and (b) on the inner surface of the innermost stressed (2nd) layer.

**Case a:** For the case where the input temperature is uniformly applied on the outermost surface of a hollow  $J$ -layer cylinder, the following boundary and interface conditions are applied.

At  $r = 0$  (center of the bore)

$$BC.1 \quad T^1(r, t) \text{ is finite}$$

At  $r = r_1$  (on the innermost surface)

$$BC.2 \quad T^1(r, t) = T^2(r, t)$$

$$BC.3 \quad k_1 \frac{\partial T^1(r, t)}{\partial r} = k_2 \frac{\partial T^2(r, t)}{\partial r}$$

$$BC.4 \quad \sigma_r^2(r, t) = 0$$

At  $r = r_j$ ,  $j = 2, 3, \dots, J-1$  (on the interfaces between layers)

$$BC.5 \quad T^j(r_j, t) = T^{j+1}(r_j, t)$$

$$BC.6 \quad k_j \frac{\partial T^j(r_j, t)}{\partial r} = k_{j+1} \frac{\partial T^{j+1}(r_j, t)}{\partial r}$$

$$BC.7 \quad u^j(r_j, t) = u^{j+1}(r_j, t)$$

$$BC.8 \quad \sigma_r^j(r_j, t) = \sigma_r^{j+1}(r_j, t)$$

At  $r = r_J$  (on the outermost surface)

$$BC.9 \quad T^J(r_J, t) - T_a(t) = 0$$

$$BC.10 \quad \sigma_r^J(r_J, t) = 0$$

where  $k_j$  is the thermal conductivity of the  $j$ th layer and  $T_a(t)$  is the input temperature.

In the above boundary conditions,  $BC.2$  and  $BC.5$  and  $BC.3$  and  $BC.6$  are the temperature and heat flux continuity conditions across the interfaces of any two adjacent layers, respectively,  $BC.4$  and  $BC.10$  imply the traction free conditions at the innermost and outermost surfaces, while  $BC.7$  and  $BC.8$  indicate the continuity of displacements and tractions at the layer interfaces, respectively.

**Case b:** For the case where the input temperature is uniformly applied to the inner surface (bore) of the cylinder, that is at  $r = r_1$ , the boundary condition  $BC.1$  is not required and  $BC.2$  is replaced by

$$BC.2a \quad T^1(r_1, t) - T_a(t) = 0$$

while the outermost surface is assumed to be insulated such that  $BC.9$  is replaced by

$$BC.9a \quad \frac{\partial T^J(r_J, t)}{\partial r} = 0$$

The other interface boundary conditions are identical to those for the case of external input temperature.

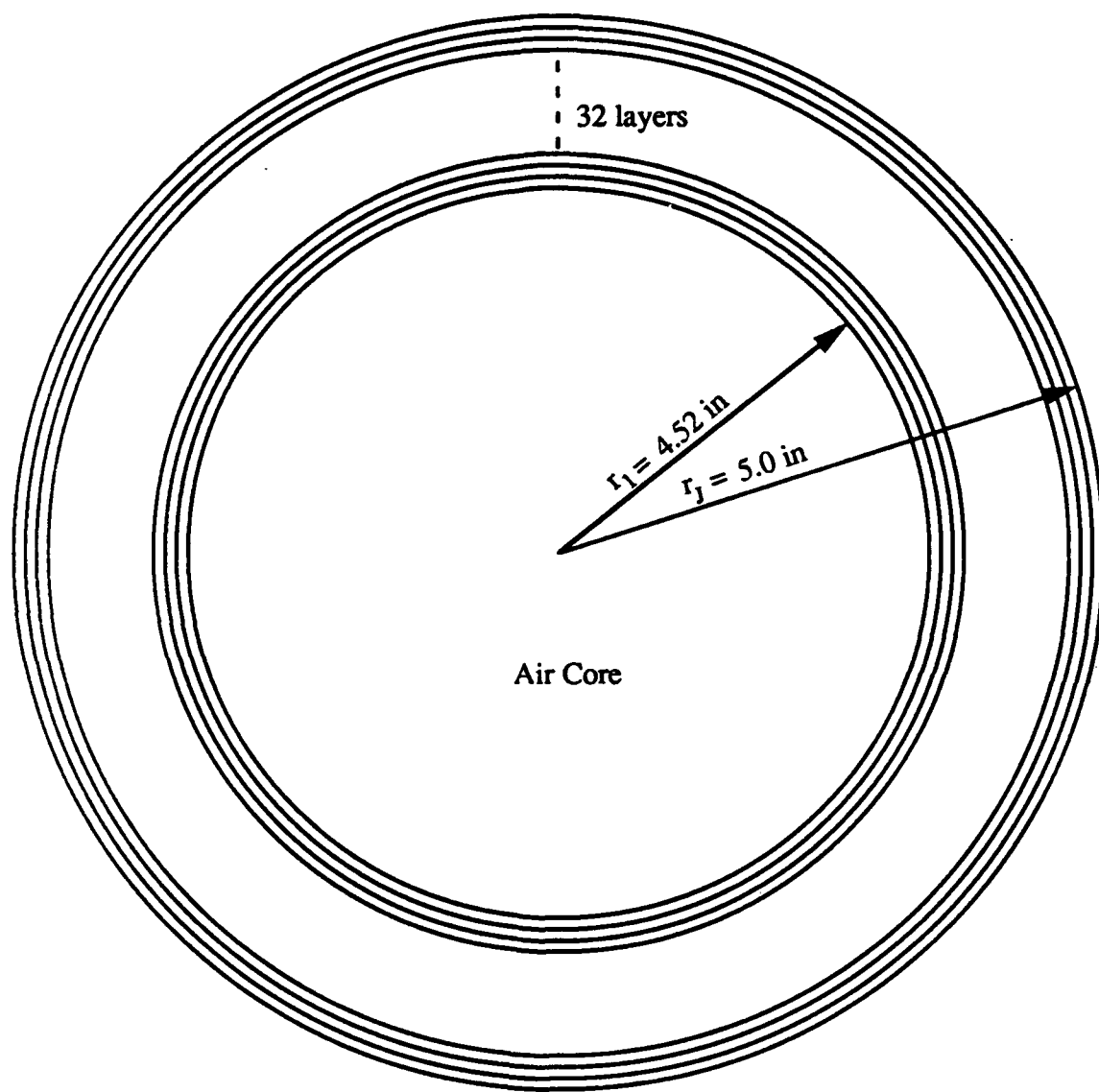


**Figure 1**  
**Configuration of the Cylinder**

## Reliability Analysis

The structural reliability analysis of the cylinder is based on the "weakest link" principle which takes into consideration both the applied stress and the effected volume of material. The probability that a unit volume of material survives under the application of a stress,  $S$ , is given as [21]

$$L(s) = \exp \left[ - \left( \frac{s}{R_c} \right)^m \right] \quad (19)$$

where  $L(s)$  is the reliability,  $R_c$  and  $m$  are the "characteristic" ultimate strength of the reference volume, and the Weibull shape parameter respectively. These two constants define the two-parameter Weibull distribution. The "characteristic strength" has a probability of survival of  $L(R_c) = e^{-1} = 0.3679$ . Survival of structural components requires that all volume elements survive. When the elements are independent of each other, the reliability of the component  $L$  is equal to the product of the individual reliabilities of volume elements (weakest link hypothesis) [22].

$$L(s_1, s_2, \dots, s_n) = \exp \left[ - \left( \frac{s_1}{R_c} \right)^m \frac{V_1}{V_r} \right] \times \exp \left[ - \left( \frac{s_2}{R_c} \right)^m \frac{V_2}{V_r} \right] \\ \times \dots \times \exp \left[ - \left( \frac{s_n}{R_c} \right)^m \frac{V_n}{V_r} \right] \quad (20)$$

where  $n$  is the total number of all the volume elements and  $V_r$  is the reference volume whose strength parameters are  $R_c$  and  $m$ . Using the common base,  $e$

$$L = \exp \left[ - \sum_{j=1}^n \left( \frac{s_j}{R_c} \right)^m \frac{V_j}{V_r} \right] \quad (21)$$

For small volume elements the summation is replaced by integration

$$L = \exp \left[ - \int_V \left( \frac{s}{R_c} \right)^m \frac{dv}{V_r} \right] \quad (22)$$

where the risk of failure,  $\lambda$ , the exponent of  $e$ , is called the stress-volume integral [23]. If  $S_{\max}$  is the maximum value of the applied stress through the component and  $V$  is its total stressed volume, Eq. 20 may be written in terms of dimensionless ratios as

$$\ln(1/L) = \lambda = \left( \frac{1}{V_c} \right)^m \frac{V}{V_r} \int_V \left( \frac{s}{S_{\max}} \right)^m \frac{dv}{V} \quad (23)$$

The integration is carried out only over the volume where stresses exist. A safety factor is introduced as follows

$$V_c = \frac{R_c}{S_{\max}}$$

Reliability function such as Eq. 23 can be written for each layer of the carbon-carbon cylinder. After the stress distribution is calculated the reliability of each concentric cylindrical layer is determined.

In cylindrical coordinates,  $dv$  is equal to  $2\pi r dr$  and hence Eq. 23 is transformed to



$$\ln(1/L) = \lambda = 2\pi \left( \frac{1}{v_c} \right)^m \frac{V}{v_r} \int_V \left( \frac{s}{S_{\max}} \right)^m \frac{rdr}{V} \quad (24)$$

Tension tests have been performed on dog bone shaped carbon-carbon composite specimens in both the warp and fill directions [1]. The specimen size (reference volume) is  $2 \times 1/4 \times 3/8$  in, or  $0.1875 \text{ in}^3$ . An average strength of  $\mu_R = 15,000$  psi was measured in the warp direction while the fill strength was 6000 psi. The coefficient of variation (COV) in both cases was 6.67%.

From these observations the shape parameter,  $m$  and the characteristic strength  $R_c$  of the reference volume is calculated as

$$m \simeq \frac{1.2}{\text{COV}} \quad (25)$$

$$R_c = \frac{\mu_R}{\Gamma(1 + \frac{1}{m})} \quad (26)$$

where  $\Gamma(\cdot)$  is the gamma function. The observed values for  $m$

$$m \simeq \frac{1.2}{0.067} = 18$$

and for the characteristic strength in the warp direction,  $R_{cw}$ , and fill direction  $R_{cf}$

$$R_{cw} = \frac{15,000}{0.9711} = 15,400 \text{ psi} \quad \text{and} \quad R_{cf} = \frac{6000}{0.9711} = 6,180 \text{ psi}$$

are obtained.

The probability of failure,  $P_{fj}$ , of a  $j$ th layer is calculated from Eq. 24 as

$$P_{fj} = 1 - L_j \quad (27)$$

The reliability of the complete structure is again based on the weakest link principle and is calculated as the product of layer reliabilities. The probability of failure of the complete structure becomes

$$P_f = 1 - \prod_{j=1}^n L_j \quad (28)$$

When all the tangential stresses in the cylinder are smaller than the characteristic strength  $R_c$  and the  $\lambda$  values are very small, then the following equation is quite accurate:

$$P_f = 1 - \prod_{j=1}^n L_j \simeq \sum_{j=1}^{n_f} \lambda_j \quad (29)$$

where  $n$  is the total number of layers.

## Illustrative Examples

When the input temperature is a harmonic function with an amplitude  $A$  and frequency  $\omega$ , such that

$$T_a(t) = A e^{i\omega t} \quad (30)$$

the response  $X(r, t)$ , such as temperature, displacement, and stresses, can be expressed in terms of the complex frequency response function as follows:

$$X = |\tilde{X}| \exp[i(\omega t + \phi)] \quad (31)$$

where  $|\tilde{X}(r, \omega)|$  and  $\phi(r, \omega)$  are the frequency dependent amplitude and phase angle of the response, respectively, and are defined as

$$\tilde{X} = A\tilde{H}, \quad \phi = \tan^{-1}(\tilde{H}_{IM}/\tilde{H}_{RE}) \quad (32)$$

with  $\tilde{H}(r, \omega) = \tilde{H}_{RE}(r, \omega) + i\tilde{H}_{IM}(r, \omega)$  the corresponding complex frequency response function for the input temperature with a unit amplitude and frequency  $\omega$ .

If the input temperature is a general function of time, then the responses (temperature, displacement, and stresses) are also some functions of time. In this case, the time response functions for temperature, displacement, and stresses are obtained via the method of Fourier transforms. The Fourier transform pair is defined as [24-25]

$$\tilde{X}(r, \omega) = \int_{-\infty}^{\infty} X(r, t) e^{-i\omega t} dt, \quad X(r, t) = \frac{1}{2\pi} \int_{-\infty}^{\infty} \tilde{X}(r, \omega) e^{i\omega t} d\omega \quad (33)$$

where  $\tilde{X}$ , in this case, is the complex function representing the product of the frequency response function and the Fourier transform of the input temperature such that

$$\tilde{X} = \tilde{H}\tilde{T}_a \quad (34)$$

for which  $\tilde{T}_a(\omega)$  is the Fourier transform of the input temperature.

For the current problem of coupled thermoelasticity, the response function  $\tilde{H}$  is a complex conjugate function with respect to  $\omega$ , that is

$$\tilde{H}_{RE}(r, -\omega) = \tilde{H}_{RE}(r, \omega) \quad \text{and} \quad \tilde{H}_{IM}(r, -\omega) = -\tilde{H}_{IM}(r, \omega) \quad (35)$$

Furthermore, if the Fourier transform of the input temperature  $\tilde{T}_a(\omega)$  is also a conjugate function with respect to the input frequency  $\omega$ , then  $X$ , as the product of  $H$  and  $T_a$ , is also a conjugate function with respect to the frequency,  $\omega$ .

$$\tilde{X}_{RE}(r, -\omega) = \tilde{X}_{RE}(r, \omega), \quad \tilde{X}_{IM}(r, -\omega) = -\tilde{X}_{IM}(r, \omega) \quad (36)$$

In this situation, the inverse Fourier transform of  $\tilde{X}$ , Eq. 22, can be rewritten as

$$X(r, t) = \frac{1}{\pi} \int_0^{\infty} [\tilde{X}_{RE}(r, \omega) \cos(\omega t) - \tilde{X}_{IM}(r, \omega) \sin(\omega t)] d\omega \quad (37)$$

where the above integral involves only real functions and can be integrated using standard numerical methods. After performing the inverse Fourier transformation, the responses, such as temperature, displacement, and stresses at any given point in the cylinder are obtained as functions of time. The advantage of using the Fourier transform technique is that it can directly utilize the existing complex frequency response functions. Furthermore, the integral for the inverse Fourier transform is simpler to obtain than that for the Laplace inverse transform.

In this section, thermal shocks are applied to a hollow thirty two layer cylinder, with two alternating layers of fiber. The geometric, thermal and mechanical parameters used are listed in Table 1 while the cylinder configuration is shown in Fig. 1. The input shock temperature is modeled as

$$T_a(t) = \begin{cases} 0 & \text{for } t \leq 0 \\ 2700\beta t e^{1-\beta t} \text{ K} & \text{for } t > 0 \end{cases} \quad (38)$$

Table 1. Geometric, Thermal and Mechanical Parameters for Isotropic Materials.

Material, $j$	Fiber Layers		
	Air	Fill Direction (z)	Warp Direction ( $\theta$ )
Thickness (in)	$r_1 = 4.52$	0.015	0.015
Conductivity, $k_j$ (Btu/hr ft <sup>2</sup> F)	0.0142	12.5	12.5
Diffusivity, $\gamma_j$ (in <sup>2</sup> /hr)	106.28	96.107	96.107
Elastic Modulus, $E_j$ (psi)	—	$1.6 \times 10^6$	$2.55 \times 10^6$
Poisson's Ratio, $\nu_j$	—	0.05	0.08
Strength, $R_{cj}$ (psi)	—	$1.6 \times 10^3$	$1.5 \times 10^4$
Coefficient of Thermal Expansion, $\alpha_j$ (in./in. <sup>2</sup> F)	—	$1.75 \times 10^{-5}$	$1.75 \times 10^{-5}$
Coupling Coefficient, $\delta_j$	—	0.0	0.0
		0.1	0.1
		0.3	0.3
		0.5	0.5

where  $\beta$  is a constant that regulates the rise time and decay of the shock. The rise time,  $t_m$ , is defined as the time required for the input temperature to reach the maximum value. In terms of the constant  $\beta$ ,  $t_m = 1/\beta$ . Thermal shock with rise time,  $t_m = 1$  second, is investigated (Fig. 2).

The Fourier transform of the input temperature function, Eq. 38, is obtained as

$$\tilde{T}_a(\omega) = 2700\beta e \left[ \frac{\beta^2 - \omega^2}{(\beta^2 + \omega^2)^2} - i \frac{2\beta\omega}{(\beta^2 + \omega^2)^2} \right] \quad (39)$$

where it is obvious that  $\tilde{T}_a$  is a complex conjugate function with respect to  $\omega$ .

#### Cylinder subjected to an internal shock

For the temperature time history (Fig. 2) applied to the innermost surface, the tangential stresses on the innermost and outermost surface are shown in Figs. 3 and 4 for different coupling coefficients  $\delta$ . The tangential stresses on the innermost surface reach the highest compressive values first, eventually stress inversion takes place; finally stresses tend to zero while the shock decays. The tangential stresses on the outermost surface reach the highest tensile values first, then they change sign and reach the highest compressive values; they also tend to zero while the shock decays. The maximum compressive stress in the cylinder occurs at the innermost surface while the maximum tensile stress occurs at the outermost surface.

The probabilities of failure of the structure, the innermost and outermost layers have been calculated as indicated in Section 2 with a coupling coefficient,  $\delta$ , of 0.1 and are presented in Fig. 5. These probabilities are influenced most by the stresses on the innermost surface. The effect of the coupling coefficient on the failure probabilities of the cylinder is shown in Fig. 6.

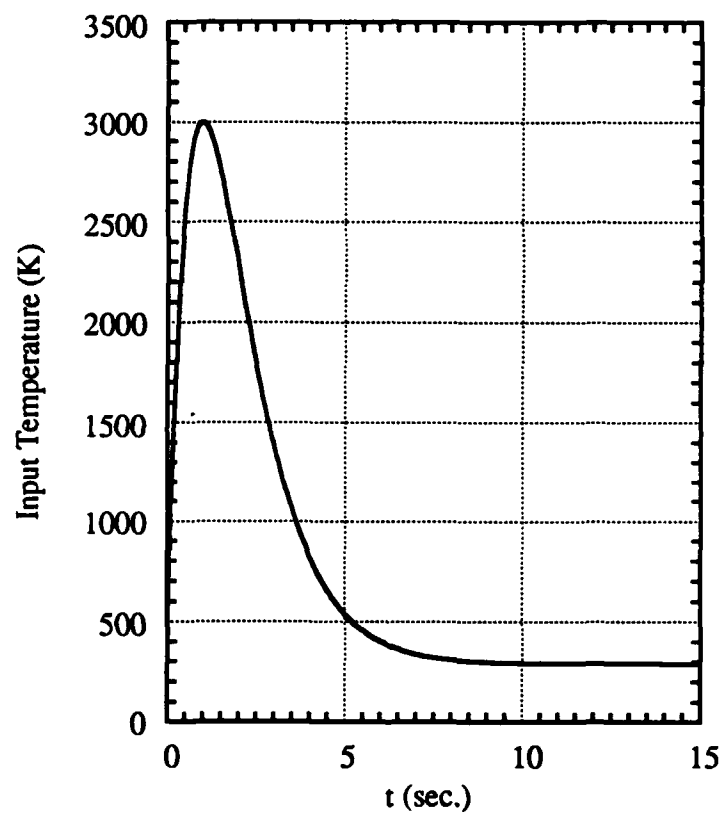


**Figure 2**  
**Input Temperature (K)**

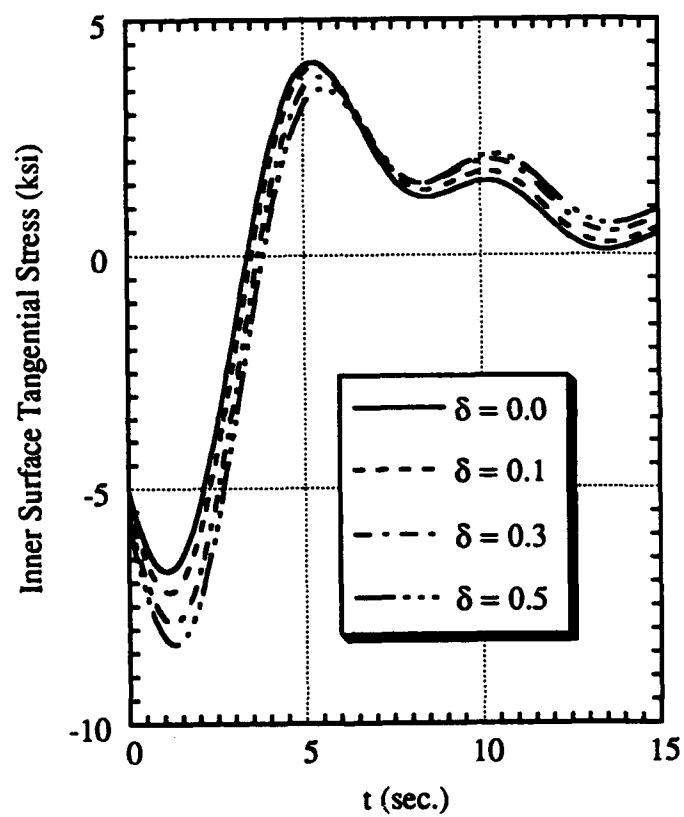


**Figure 3**  
**Tangential Stress on the Innermost Surface under Internal Thermal Shock**

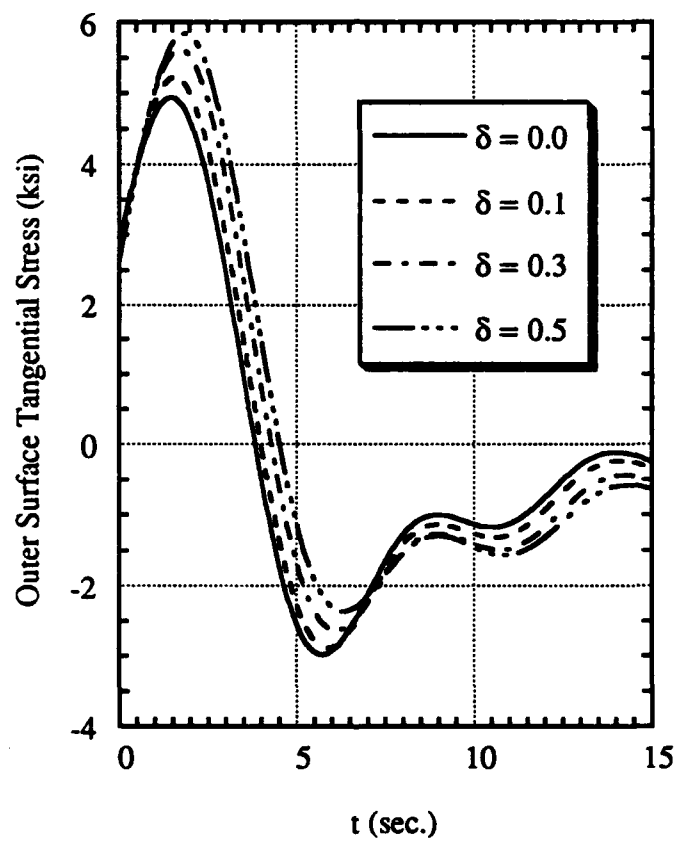


**Figure 4**  
**Tangential Stress on the Outermost Surface under Internal Thermal Shock**

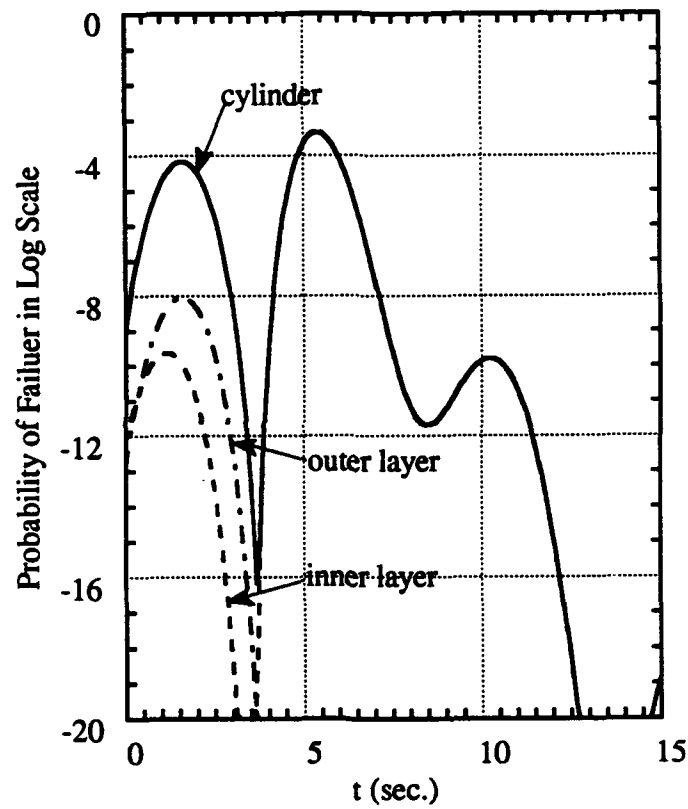


**Figure 5**  
**Probability of Failure of the Cylinder, Innermost and Outermost Layer, under Internal Thermal Shock**

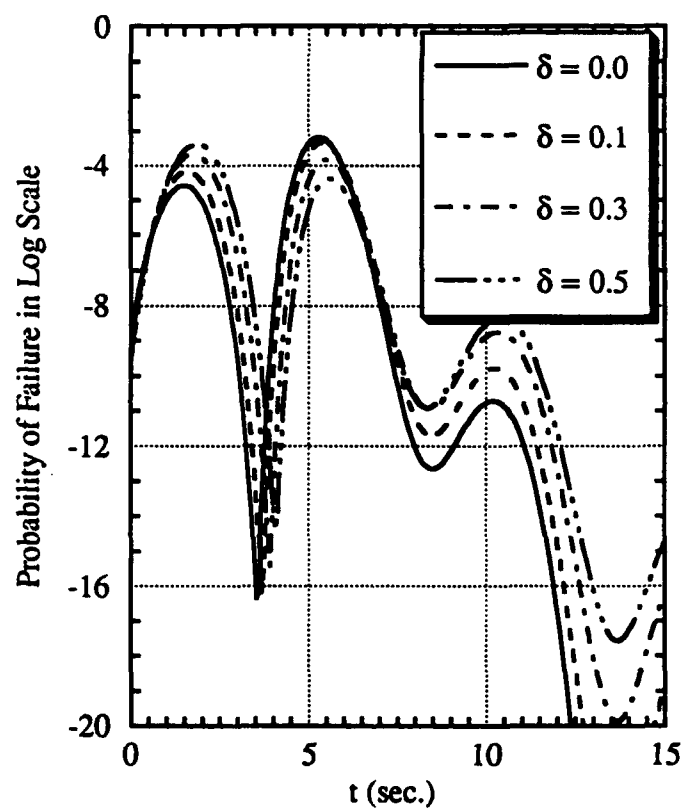


**Figure 6**  
**Probability of Failure of the Cylinder, for Different Coupling Coefficients, under Internal Thermal Shock**



#### **Cylinder subjected to an external shock**

For the same temperature time history applied to the outermost surface, the tangential stresses are presented in Figs. 7 and 8. The tangential stresses on the innermost surface reach the highest tensile values first, then they change sign and subsequently reach the highest compressive values, finally tending to zero while the shock decays. The tangential stresses on the outermost surface reach the highest compressive values first, then they change sign and reach the highest tensile values, again tending to zero while the shock decays. As with the internal shock, the maximum compressive stresses are greater than the tensile ones, but, on the contrary, the maximum compressive stresses occur at the outermost surface while the maximum tensile stresses occur at the innermost surface.

The probabilities of failure of the structure, the innermost and outermost layers have been calculated and plotted in Fig. 9 for a coupling coefficient,  $\delta$ , of 0.1. These probabilities are influenced most by the stresses on the outermost surfaces. It is seen that the two highly stressed layers on the two surfaces of the cylinder contribute most to the probability of failure. The effect of the coupling coefficient on the failure probabilities of the cylinder is shown in Fig. 10.

Figs. 3, 4, 7 and 8 show the evident differences of tangential stresses for different coupling coefficients. When the coupling coefficients are larger, the maximum tangential stresses are larger. The coupling coefficients have similar effects on the probabilities of failure, hence it is very important to study these effects when the coupling coefficient,  $\delta$ , is large. Some typical coupling coefficients are presented in Table 2 for various materials.

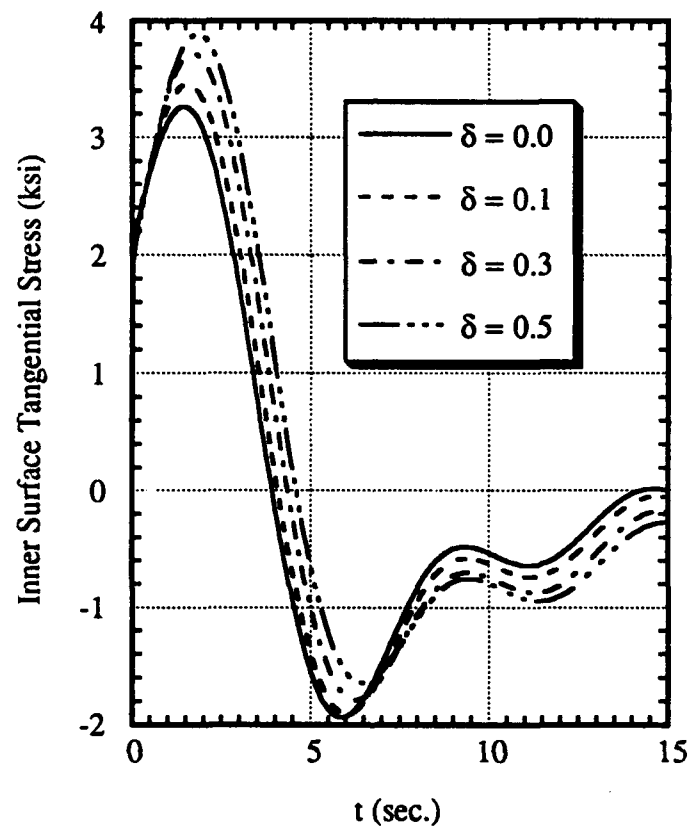


**Figure 7**  
**Tangential Stress on the Innermost Surface under External Thermal Shock**

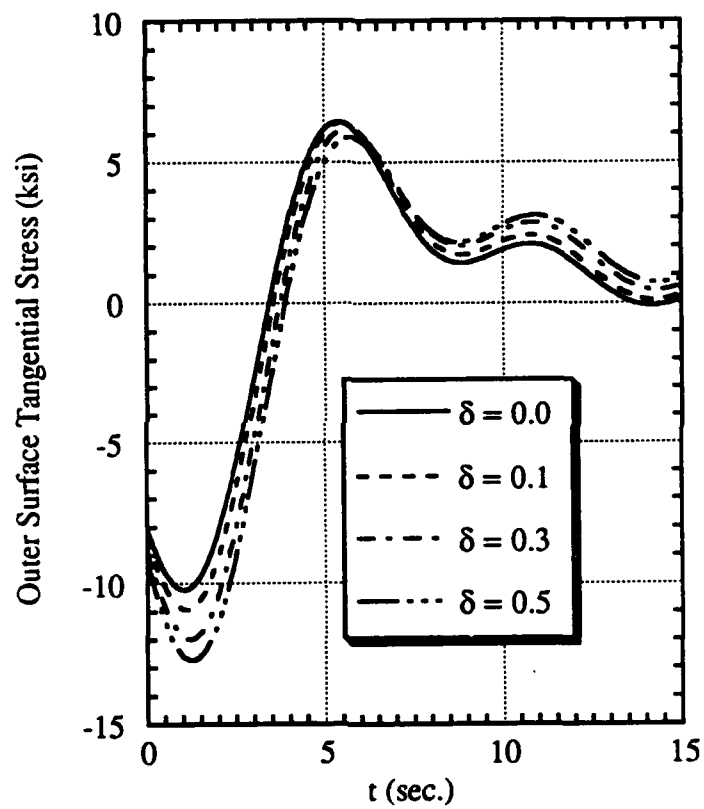


**Figure 8**  
**Tangential Stress on the Outermost Surface under External Thermal Shock**

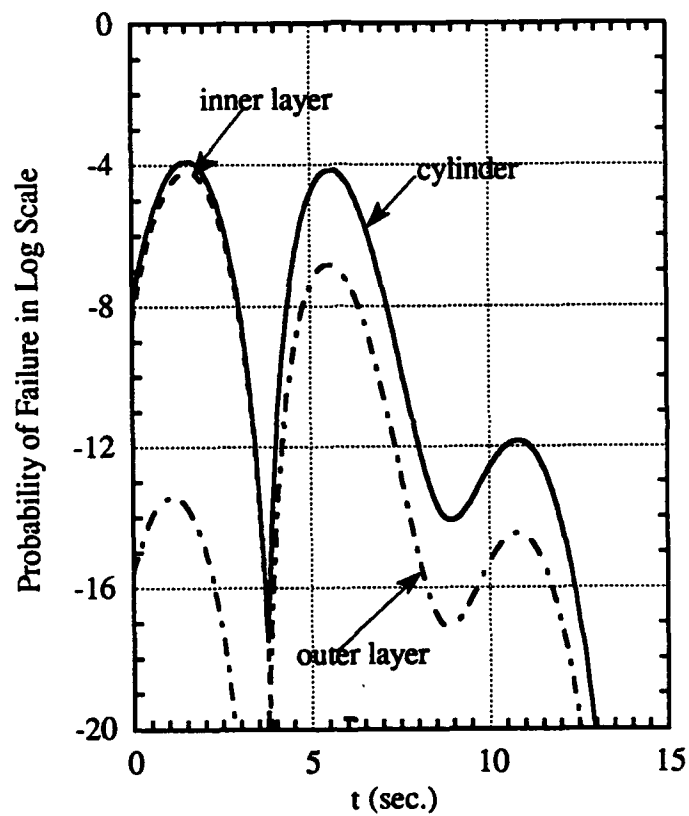


**Figure 9**  
**Probability of Failure of the Cylinder, Innermost and Outermost Layer, under External Thermal Shock**

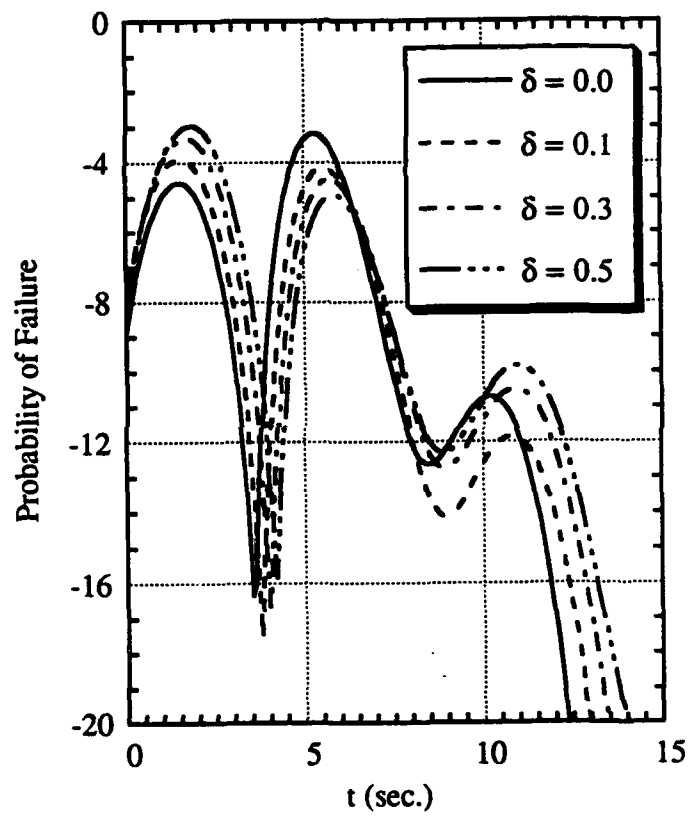


**Figure 10**  
**Probability of Failure of the Cylinder, for Different Coupling Coefficients, under External Thermal Shock**

**Table 2. Coupling Coefficients of Some Engineering Materials[26-28]**

Material	Elastic Modulus (GPa)	Poisson's Ratio	Thermal Expansion Coeff. $\times 10^{-6}$ , (mm/mm/°K)	Specific Gravity	Specific Heat (cal/kg/°K)	Coupling Coeff.
Aluminum	69.0	0.35	25.2	2.70	215.	0.0374
Copper	124.	0.37	16.6	8.96	92.0	0.0248
Lead	15.9	0.45	28.8	11.4	31.0	0.0706
Steel	207.	0.30	12.1	7.86	108.	0.0118
Polystyrene	4.14	0.45	80.0	1.04	320.	0.15
Polyvinylchloride and Vinylchloride Acetate	4.14	0.40	180.	1.36	200.	0.412
Carbon	17.2	0.08	31.5	1.50	38.0	0.0304
Graphite Fiber	243.	0.32	16.8	0.96	170.	0.162
Kevlar Fiber	152.	0.35	54.0	0.85	250.	1.03
Polyurethane	$5.5 \times 10^{-3}$	0.49	153.	1.67	368.	0.0022

$T_R = 300.0^\circ\text{K}$

$1 \text{ N}\cdot\text{m} = 1 \text{ J} = 0.239 \text{ cal}$

mass density  $\rho$  (Kg/m<sup>3</sup>) = 1000.0x Specific Gravity

## SECTION 3. ORTHOTROPIC CYLINDER PROBLEM

### Temperature Analysis

It has been illustrated in Section 2 that for small coupling coefficients the uncoupled thermal stress analysis is sufficiently accurate. The carbon-carbon composite has a coupling coefficient of  $\delta = 0.0304$  (Table 2), hence in the following, uncoupled analysis is used. The heat conduction equation for an orthotropic material is given as follows:

$$\gamma_{11} \left( \frac{\partial^2 T}{\partial r^2} + \frac{1}{r} \frac{\partial T}{\partial r} \right) + \gamma_{22} \frac{1}{r^2} \frac{\partial^2 T}{\partial \theta^2} = \frac{\partial T}{\partial t} \quad (40)$$

where  $T(r, \theta, t)$  is the temperature function,  $r$  and  $\theta$  are the radial and tangential coordinates, and  $t$  is time,  $\gamma_{11}$  and  $\gamma_{22}$  are the coefficients of radial and tangential thermal diffusivities, respectively.

Expanding the temperature in the  $j$ th layer into Fourier series:

$$T(r, \theta, t) = \sum_{n=-\infty}^{\infty} T_n(r, t) e^{in\theta} \quad (41)$$

Assuming zero initial condition for the temperature is  $T(r, \theta, 0) = 0$ , substituting Eq. 41 into Eq. 40, and applying the Laplace transform to it, the heat conduction equation becomes:

$$\gamma_{11} \left( \frac{\partial^2 \tilde{T}_n}{\partial r^2} + \frac{1}{r} \frac{\partial \tilde{T}_n}{\partial r} \right) - \left( \gamma_{22} \frac{n^2}{r^2} + s \right) \tilde{T}_n = 0 \quad (42)$$

where  $\tilde{T}_n$  is the Laplace transform of  $T_n$  in Eq. 41. Solving Eq. 42, the temperature in Laplace transform domain can be obtained in terms of the modified Bessel functions  $I_\nu(x)$  and  $K_\nu(x)$  as follows:

$$\tilde{T}_n = \tilde{T}_{n1} I_{\nu_n}(ar) + \tilde{T}_{n2} K_{\nu_n}(ar) \quad (43)$$

$$a = \sqrt{\frac{s}{\gamma_{11}}} \quad \text{and} \quad \nu_n = n \sqrt{\frac{\gamma_{22}}{\gamma_{11}}}$$

where  $\tilde{T}_{n1}$  and  $\tilde{T}_{n2}$  are constants to be determined by the following temperature boundary conditions.

**Case a:** The input temperature is uniformly applied on the outermost surface of a hollow  $J$ -layered cylinder:

At  $r = 0$  (center of the bore)

$$BC.1 \quad \tilde{T}^1(r, \theta, t) \text{ is finite}$$

At  $r = r_j$ ,  $j = 1, 2, 3, \dots, J - 1$  (on the interfaces between layers)

$$BC.2 \quad \tilde{T}^j(r, \theta, t) = \tilde{T}^{j+1}(r, \theta, t)$$

$$BC.3 \quad k_{rj} \frac{\partial \tilde{T}^j(r, \theta, t)}{\partial r} = k_{j+1} \frac{\partial \tilde{T}_{j+1}(r, \theta, t)}{\partial r}$$

At  $r = r_J$  (on the outermost surface)

$$BC.4 \quad \tilde{T}^J(r, \theta, t) - \tilde{T}_a(\theta, t) = 0$$

**Case b:** The input temperature is uniformly applied on the innermost surface of a hollow  $J$ -layered cylinder:

At  $r = r_1$  (on the innermost surface)

$$BC.1 \quad \tilde{T}^1(r, \theta, t) = \tilde{T}_a(\theta, t)$$

At  $r = r_{j+1}$ ,  $j = 1, 2, 3, \dots, J - 1$  (on the interfaces between layers)

$$BC.2 \quad \tilde{T}^j(r, \theta, t) = \tilde{T}^{j+1}(r, \theta, t)$$

$$BC.3 \quad k_{rj} \frac{\partial \tilde{T}^j(r, \theta, t)}{\partial r} = k_{j+1} \frac{\partial \tilde{T}_{j+1}(r, \theta, t)}{\partial r}$$

At  $r = r_J$  (on the outermost surface)

$$BC.4 \quad \frac{\partial \tilde{T}^J(r, \theta, t)}{\partial r} = 0$$

where  $\tilde{T}_a(\theta, t)$  is the Laplace transform of the input temperature on the outermost surface. The temperature can be obtained as the inverse Laplace transform of Eq. 43.

## Stress Analysis

Equilibrium equations for a plane strain problem in cylindrical coordinates are given as:

$$\begin{aligned} \frac{\partial \sigma_r}{\partial r} + \frac{1}{r} (\sigma_r - \sigma_\theta) + \frac{1}{r} \frac{\partial \tau_{r\theta}}{\partial \theta} &= 0 \\ \frac{\partial \tau_{r\theta}}{\partial r} + \frac{1}{r} \frac{\partial \sigma_\theta}{\partial \theta} + \frac{2}{r} \tau_{r\theta} &= 0 \end{aligned} \quad (44)$$

where  $\sigma_r(r, \theta, t)$ ,  $\sigma_\theta(r, \theta, t)$  and  $\tau_{r\theta}(r, \theta, t)$  are the radial, tangential and shear stress components, respectively.

The stress-strain relationships for an orthotropic plane strain problem are:

$$\begin{aligned} \sigma_r &= C_{11} \epsilon_r + C_{12} \epsilon_\theta - \beta_1 T \\ \sigma_\theta &= C_{12} \epsilon_r + C_{22} \epsilon_\theta - \beta_2 T \\ \tau_{r\theta} &= C_{66} \gamma_{r\theta} \end{aligned} \quad (45)$$

where  $\epsilon_r(r, \theta, t)$ ,  $\epsilon_\theta(r, \theta, t)$  and  $\gamma_{r\theta}$  are radial, circumference, and shear strain, respectively.  $C_{ij}$ ,  $i, j = 1, 2, 3, 6$  are Hook's constants;  $\beta_1$ , and  $\beta_2$  are defined in terms of Hook's constants and coefficients of thermal expansion  $\alpha_r$ ,  $\alpha_\theta$  and  $\alpha_z$  in the radial, tangential and axial directions respectively, as:



$$\beta_1 = C_{11} \alpha_r + C_{12} \alpha_\theta + C_{13} \alpha_z$$

$$\beta_2 = C_{12} \alpha_r + C_{22} \alpha_\theta + C_{23} \alpha_z$$

The strain-displacement relations for a plane strain problem in cylindrical coordinates are:

$$\begin{aligned} \epsilon_r &= \frac{\partial u}{\partial r}, & \epsilon_\theta &= \frac{1}{r} \left( \frac{\partial v}{\partial \theta} + u \right) \\ \gamma_{r\theta} &= \frac{1}{r} \left( \frac{\partial u}{\partial \theta} + r \frac{\partial v}{\partial r} \right) \end{aligned} \quad (46)$$

where  $u(r, \theta, t)$  is radial displacement and  $v(r, \theta, t)$  is circumferential displacement. Substituting Eqs. 45 and 46 into 44, the equilibrium equations for a plane strain problem in cylindrical coordinates can be rewritten in terms of displacements in the following form:

$$\begin{aligned} C_{11} \left( \frac{\partial^2 u}{\partial r^2} + \frac{1}{r} \frac{\partial u}{\partial r} \right) + C_{66} \frac{1}{r^2} \frac{\partial^2 u}{\partial \theta^2} - C_{22} \frac{u}{r^2} + (C_{12} + C_{66}) \frac{1}{r} \frac{\partial^2 v}{\partial r \partial \theta} \\ - (C_{22} + C_{66}) \frac{1}{r^2} \frac{\partial v}{\partial \theta} - f_r = 0 \\ C_{66} \left( \frac{\partial^2 v}{\partial r^2} + \frac{1}{r} \frac{\partial v}{\partial r} \right) + C_{22} \frac{1}{r^2} \frac{\partial^2 v}{\partial \theta^2} - C_{66} \frac{v}{r^2} + (C_{12} + C_{66}) \frac{1}{r} \frac{\partial^2 u}{\partial r \partial \theta} \\ + (C_{22} + C_{66}) \frac{1}{r^2} \frac{\partial u}{\partial \theta} - f_\theta = 0 \end{aligned} \quad (47)$$

where

$$f_r = \beta_1 \frac{\partial T}{\partial r} + (\beta_1 - \beta_2) \frac{T}{r}$$

$$f_\theta = \beta_2 \frac{1}{r} \frac{\partial T}{\partial \theta}$$

Because of  $f_r$  and  $f_\theta$ , radial displacement,  $u$ , and tangential displacement,  $v$ , contain homogeneous and particular parts of the solutions of Eq. 47. Expanding them into Fourier series:

$$u = \sum_{n=-\infty}^{\infty} (u_n + u_{pn}) e^{in\theta}, \quad v = \sum_{n=-\infty}^{\infty} (v_n + v_{pn}) e^{in\theta} \quad (48)$$

The homogeneous solutions are as follows

$$\text{for } n = 0 \quad u_0 = u_{01} r^{\lambda_{01}} + u_{02} r^{-\lambda_{01}}, \quad v_0 \equiv 0 \quad (49)$$

where  $\lambda_{01}$  is defined as

$$\lambda_{01} = \sqrt{\frac{C_{22}}{C_{11}}}$$

$$\begin{aligned} \text{for } n = 1 \quad u_1 &= u_{11} + u_{12} \ln r + u_{13} r^{\lambda_{11}} + u_{14} r^{-\lambda_{11}} \\ v_1 &= v_{11} + v_{12} \ln r + v_{13} r^{\lambda_{11}} + v_{14} r^{-\lambda_{11}} \end{aligned} \quad (50)$$

where

$$\lambda_{11} = \sqrt{\frac{C_{11}C_{22} - 2C_{12}C_{66} - (C_{12})^2 + (C_{11} + C_{22})C_{66}}{C_{11}C_{66}}}$$

and

$$v_{11} = i \left( u_{11} + \frac{C_{12} + C_{66}}{C_{22} + C_{66}} u_{12} \right)$$

$$v_{12} = i u_{12}$$

$$v_{13} = i \frac{C_{22} + C_{66} - C_{11}(\lambda_{11})^2}{C_{22} + C_{66} - (C_{12} + C_{66})\lambda_{11}} u_{13}$$

$$v_{14} = i \frac{C_{22} + C_{66} - C_{11}(\lambda_{11})^2}{C_{22} + C_{66} + (C_{12} + C_{66})\lambda_{11}} u_{14}$$

$$\text{for } n > 1 \quad u_n = \sum_{m=1}^4 u_{nm} r^{\lambda_{nm}}, \quad v_n = \sum_{m=1}^4 v_{nm} r^{\lambda_{nm}} \quad (51)$$

where  $\lambda_{nm}$  are the roots of the following equation

$$C_{11}C_{66}(\lambda_n)^4 - [(C_{11}C_{22} - 2C_{12}C_{66} - (C_{12})^2)n^2 + (C_{11} + C_{22})C_{66}](\lambda_n)^2 + C_{22}C_{66}(n^2 - 1)^2 = 0$$

and

$$v_n = \frac{i}{n} \sum_{m=1}^4 \frac{C_{22} + C_{66}n^2 - C_{11}(\lambda_{nm})^2}{C_{22} + C_{66} - (C_{12} + C_{66})\lambda_{nm}} u_{nm} r^{\lambda_{nm}}$$

The particular solutions can be obtained by the method of variation of parameters. Substituting the solutions for displacements back into the strain-displacement relationship Eq. 46 and stress-strain relationship Eq. 45, the stresses can be obtained as follows

$$\begin{aligned} \sigma_{r0} &= (C_{12} + C_{11}\lambda_{01})r^{\lambda_{01}-1}u_{01} + (C_{12} - C_{11}\lambda_{01})r^{-\lambda_{01}-1}u_{02} \\ &\quad + C_{11}\frac{\partial u_{p0}}{\partial r} + in\frac{C_{12}}{r}v_{p0} + \frac{C_{12}}{r}u_{p0} - \beta_1 T_0 \\ \sigma_{\theta 0} &= (C_{22} + C_{12}\lambda_{01})r^{\lambda_{01}-1}u_{01} + (C_{22} - C_{12}\lambda_{01})r^{-\lambda_{01}-1}u_{02} \\ &\quad + C_{12}\frac{\partial u_{p0}}{\partial r} + in\frac{C_{22}}{r}v_{p0} + \frac{C_{22}}{r}u_{p0} - \beta_2 T_0 \end{aligned} \quad (52)$$

$$\tau_{r\theta 0} \equiv 0$$

$$\sigma_{r1} = \left( C_{11} - C_{22} \frac{C_{12} + C_{66}}{C_{22} + C_{66}} \right) \frac{u_{12}}{r}$$

$$\begin{aligned}
& -\lambda_{11} \frac{C_{12}(C_{12} + C_{66}) - C_{11}(C_{22} + C_{66}) + C_{11}C_{66}\lambda_{11}}{C_{22} + C_{66} - (C_{12} + C_{66})\lambda_{11}} r^{\lambda_{11}-1} u_{13} \\
& + \lambda_{11} \frac{C_{12}(C_{12} + C_{66}) - C_{11}(C_{22} + C_{66}) - C_{11}C_{66}\lambda_{11}}{C_{22} + C_{66} + (C_{12} + C_{66})\lambda_{11}} r^{-\lambda_{11}-1} u_{14} \\
& + C_{11} \frac{du_{p1}}{dr} + inC_{12} \frac{v_{p1}}{r} + C_{12} \frac{u_{p1}}{r} - \beta_1 T_1 \\
\sigma_{\theta 1} = & \left( C_{12} - C_{22} \frac{C_{12} + C_{66}}{C_{22} + C_{66}} \right) \frac{u_{12}}{r} \\
& - \lambda_{11} \frac{C_{66}(C_{22} - C_{12}) + (C_{12}^2 + C_{12}C_{66} - C_{11}C_{22})\lambda_{11}}{C_{22} + C_{66} - (C_{12} + C_{66})\lambda_{11}} r^{\lambda_{11}-1} u_{13} \\
& + \lambda_{11} \frac{C_{66}(C_{22} - C_{12}) - (C_{12}^2 + C_{12}C_{66} - C_{11}C_{22})\lambda_{11}}{C_{22} + C_{66} + (C_{12} + C_{66})\lambda_{11}} r^{-\lambda_{11}-1} u_{14} \\
& + C_{12} \frac{du_{p1}}{dr} + inC_{22} \frac{v_{p1}}{r} + C_{22} \frac{u_{p1}}{r} - \beta_2 T_1 \\
\tau_{r\theta 1} = & iC_{66} \left( 1 - \frac{C_{12} + C_{66}}{C_{22} + C_{66}} \right) \frac{u_{12}}{r} \\
& + i\lambda_{11} \frac{C_{12}(C_{12} + C_{66}) - C_{11}(C_{22} + C_{66}) + C_{11}C_{66}\lambda_{11}}{C_{22} + C_{66} - (C_{12} + C_{66})\lambda_{11}} r^{\lambda_{11}-1} u_{13} \\
& - i\lambda_{11} \frac{C_{12}(C_{12} + C_{66}) - C_{11}(C_{22} + C_{66}) - C_{11}C_{66}\lambda_{11}}{C_{22} + C_{66} + (C_{12} + C_{66})\lambda_{11}} r^{-\lambda_{11}-1} u_{14} \\
& + C_{66} \left( i \frac{u_{p1}}{r} - \frac{v_{p1}}{r} + \frac{dv_{p1}}{dr} \right)
\end{aligned} \tag{53}$$

for  $n > 1$

$$\begin{aligned}
\sigma_{rn} = & \sum_{m=1}^4 \left[ C_{11}\lambda_{nm} + C_{12} \left( 1 - \frac{C_{22} + C_{66}n^2 - C_{11}(\lambda_{nm})^2}{C_{22} + C_{66} - (C_{12} + C_{66})\lambda_{nm}} \right) \right] r^{\lambda_{nm}-1} u_{nm} \\
& + C_{11} \frac{du_{pn}}{dr} + inC_{12} \frac{v_{pn}}{r} + C_{12} \frac{u_{pn}}{r} - \beta_1 T_n \\
\sigma_{\theta n} = & \sum_{m=1}^4 \left[ C_{12}\lambda_{nm} + C_{22} \left( 1 - \frac{C_{22} + C_{66}n^2 - C_{11}(\lambda_{nm})^2}{C_{22} + C_{66} - (C_{12} + C_{66})\lambda_{nm}} \right) \right] r^{\lambda_{nm}-1} u_{nm} \\
& + C_{12} \frac{du_{pn}}{dr} + inC_{22} \frac{v_{pn}}{r} + C_{22} \frac{u_{pn}}{r} - \beta_2 T_n
\end{aligned} \tag{54}$$

$$\tau_{r\theta n} = iC_{66} \sum_{m=1}^4 \left[ n + \frac{1 + \lambda_{nm}}{n} \frac{C_{22} + C_{66}n^2 - C_{11}(\lambda_{nm})^2}{C_{22} + C_{66} - (C_{12} + C_{66})\lambda_{nm}} \right] r^{\lambda_{nm}-1} u_{nm} \\ + C_{66} \left( in \frac{u_{pn}}{r} - \frac{v_{pn}}{r} + \frac{dv_{pn}}{dr} \right)$$

The constants  $u_{nm}$  can be defined by the following boundary conditions  
At  $r = r_1$  (on the innermost surface)

$$BC.1 \quad \sigma_r^2(r_1, \theta, t) = 0$$

$$BC.2 \quad \tau_{r\theta}^2(r_1, \theta, t) = 0$$

At  $r = r_j$ ,  $j = 2, 3, \dots, J-1$  (on the interfaces between layers)

$$BC.3 \quad u^j(r_j, \theta, t) = u^{j+1}(r_j, \theta, t)$$

$$BC.4 \quad v^j(r_j, \theta, t) = v^{j+1}(r_j, \theta, t)$$

$$BC.5 \quad \sigma_r^j(r_j, \theta, t) = \sigma_r^{j+1}(r_j, \theta, t)$$

$$BC.6 \quad \tau_{r\theta}^j(r_j, \theta, t) = \tau_{r\theta}^{j+1}(r_j, \theta, t)$$

At  $r = r_J$  (on the outermost surface)

$$BC.7 \quad \sigma_r^J(r_J, \theta, t) = 0$$

$$BC.8 \quad \tau_{r\theta}^J(r_J, \theta, t) = 0$$

## Reliability Analysis

The structural reliability analysis of the cylinder is again based on the "weakest link" principle which takes into consideration both the applied stress and the effected volume of material. The probability that a reference volume  $v_r$  of material survives under the application of a stress,  $s$ , is given as [21]

$$L(s) = \exp \left[ - \left( \frac{s - R_0}{R_c - R_0} \right)^m \right] \quad (55)$$

where  $L(s)$  is the probability,  $R_c$ ,  $R_0$  and  $m$  are the characteristic ultimate strength of the reference volume,  $v_r$ , the minimum strength established by quality control and the Weibull shape parameter, respectively. These three constants define the three-parameter Weibull distribution. The characteristic strength has a probability of survival of  $L(R_c) = e^{-1} = 0.3679$ . Survival of structural components requires that all volume elements survive. When the elements are independent of each other, the reliability,  $L$ , of the component is equal to the product of the individual reliabilities of volume elements (weakest link hypothesis) [22].

$$L(s_1, s_2, \dots, s_n) = \exp \left[ - \left( \frac{s_1 - R_0}{R_c - R_0} \right)^m \frac{V_1}{v_r} \right] \times \exp \left[ - \left( \frac{s_2 - R_0}{R_c - R_0} \right)^m \frac{V_2}{v_r} \right]$$

$$\times \dots \times \exp \left[ - \left( \frac{s_n - R_0}{R_c - R_0} \right)^m \frac{V_n}{V_r} \right] \quad (56)$$

or using the common base e

$$L = \exp \left[ - \sum_{j=1}^n \left( \frac{s_j - R_0}{R_c - R_0} \right)^m \frac{V_j}{V_r} \right] \quad (57)$$

For small volume elements the summation is replaced by integration

$$L = \exp \left[ - \int_V \left( \frac{s - R_0}{R_c - R_0} \right)^m \frac{dv}{V_r} \right] \quad (58)$$

where the risk of failure,  $\lambda$ , the exponent of e, is called the stress-volume integral [23]. If  $S_{\max}$  is the maximum value of the applied stress through the component and  $V$  is its total volume, Eq. 58 may be written in terms of dimensionless ratios as

$$\ln(1/L) = \lambda = \left( \frac{1}{v_c(1 - 1/v_{\max})} \right)^m \frac{V}{V_r} \int_{s > R_0} \left( \frac{s}{S_{\max}} - \frac{v_c}{v_{\max}} \right)^m \frac{dv}{V} \quad (59)$$

The integration is carried out only over the volume where stresses exceed  $R_0$  [29]. Two safety factors are introduced as follow

$$v_c = \frac{R_c}{S_{\max}} \quad \text{and} \quad v_{\max} = \frac{R_c}{R_0}$$

Reliability functions such as Eq. 59 can be written for each layer of the carbon-carbon cylinder. After the stress distribution is calculated the reliability of each concentric cylindrical layers is determined.

In cylindrical coordinates,  $dv$  is equal to  $2\pi r dr$  and hence Eq. 59 is transformed to

$$\ln(1/L) = \lambda = 2\pi \left( \frac{1}{v_c(1 - 1/v_{\max})} \right)^m \frac{V}{V_r} \int_{s > R_0} \left( \frac{s}{S_{\max}} - \frac{v_c}{v_{\max}} \right)^m \frac{r dr}{V} \quad (60)$$

Tension tests have been performed on dog bone shaped specimens in both the warp and fill directions [1]. The specimen size (reference volume) is  $2 \times 1/4 \times 3/8$  in, or  $0.1875 \text{ in}^3$ . It is assumed here that the tensile strength and the compressive strength of the carbon-carbon composite are the same. An average strength of  $\bar{R} = 15,000$  psi was measured in the warp direction (circumferential) while the fill strength was 6000 psi (longitudinal) for carbon-carbon composite. The strength of the fiber layers in circumferential direction,  $\bar{R}_f = 24,800$  psi, is calculated based on the strengths of the composite [1], while the strength of the matrix layers,  $\bar{R}_m$  is estimated as 2,000 psi. The characteristic strength  $R_c$  and the minimum strength  $R_0$  are calculated as follows

$$R_c = r_c \bar{R} \quad \text{and} \quad R_0 = r_0 \bar{R}$$

where  $r_c = 1.03$  and  $r_0 = 0.61$ . The Weibull shape parameter,  $m$ , for both fiber layers and matrix layers is estimated as 6.17 [1]. The characteristic strength for the fiber and the matrix layers are  $R_{cf} = 25,544$  psi, and  $R_{cm} = 2,060$  psi. The minimum strength for the fiber and the matrix layers are  $R_{0f} = 15,128$  psi and  $R_{0m} = 1,220$  psi.

The probability of failure,  $P_f$ , of an individual layer is calculated from Eq. 60 as

$$P_{fj} = 1 - L_j \quad (61)$$

The reliability of the complete structure is again based on the "weakest link" principle and is calculated as the product of layer reliabilities. Again the probability of failure of the complete structure becomes

$$P_f = 1 - \prod_{j=1}^n L_j \quad (62)$$

## Illustrative Examples

### The effect of the material properties on thermal stress distributions and reliabilities

For orthotropic materials, there are nine independent mechanical constants, and three coefficients of thermal expansion compared to two mechanical constants and one coefficient of thermal expansion for isotropic materials. The following example shows how the material properties effect stress and reliability distributions of a hollow cylinder subjected to thermal loading. The cylinder consists of thirty three layers with matrix and fiber layers alternating. The thicknesses of layers 1 and 33 are half of the thickness of the rest of the layers. The geometric, mechanical and thermal parameters are listed in Table 3 while the cylinder configuration is shown in Fig. 11. The input temperature is applied at the innermost surface of the cylinder and is modeled as

$$T_a(t) = \begin{cases} 0 & \text{for } t \leq 0 \\ 3000\beta t e^{-\beta t} \text{ } ^\circ\text{F} & \text{for } t > 0 \end{cases} \quad (63)$$

where the rise time  $t_m = 1/\beta = 1$  second in this example.

To save computing time, it is assumed that the temperature is the same as the input temperature everywhere in the cylinder. The radial stresses are very small compared with the tangential stresses in the problem, and will not contribute to the failure of the structure. Fig. 12 shows the tangential stresses in layers 1 and 2 at the inner surface and in layers 32 and 33 at the outer surface (Case 1), when both the fiber and matrix materials of the cylinder are isotropic and have the same Poisson's ratios and coefficients of thermal expansion ( $\nu_{rf} = \nu_{rz} = \nu_{\theta r} = \nu_m = 0.33$ ,  $\alpha_{rf} = \alpha_{\theta r} = \alpha_{rz} = \alpha_m = 2.30 \times 10^{-6}$  in/in  $^\circ\text{F}$ ). The only difference between fiber and matrix materials is their elastic moduli ( $E_{rf} = E_{\theta r} = E_{rz} = 2.5 \times 10^6$  psi,  $E_m = 0.5 \times 10^6$  psi). The tangential stresses in this case are very small and the stresses in the fiber layers are about five times larger than the stresses in the matrix layers, just as the elastic modulus in the fiber layers is about five times larger than the modulus in the matrix layers.

As a parametric study, the moduli of the fiber layers are changed to those of carbon-carbon ( $E_{rf} = 0.86 \times 10^6$  psi,  $E_{\theta r} = 3.78 \times 10^6$  psi, and  $E_{rz} = 2.79 \times 10^6$  psi) and the rest of the material properties are kept as in Case 1 above (Case 2). Fig. 13 shows that the tangential stresses in the same locations as above are increased a little and the tangential stresses in the fiber layers are still much larger than the stresses in the matrix layers.

Next, the Poisson's ratios of the fiber layers are changed to that of carbon-carbon ( $\nu_{rf} = 0.2$ ,  $\nu_{rz} = 0.4$ ,  $\nu_{\theta r} = 0.05$ ), keeping the elastic moduli in the fiber layers as those of carbon-carbon, and the rest of the material properties as in Case 1. In this Case 3, Fig. 14 shows that the tangential stresses in the cylinder are much larger than in the above two cases, and the tangential stresses in the matrix layers are almost as large as the tangential stresses in the fiber layers even though the elastic moduli in the fiber layers are still much larger than the modulus in the matrix layers.

Finally, all the material properties including coefficients of thermal expansion in the fiber layers are chosen as those of carbon-carbon (Table 3), and the material properties in the matrix layers are kept as in Case 1. Fig. 15 shows that the tangential stress distributions are similar in this Case 4 to Case 3 presented in Fig. 14, but the tangential stresses are even

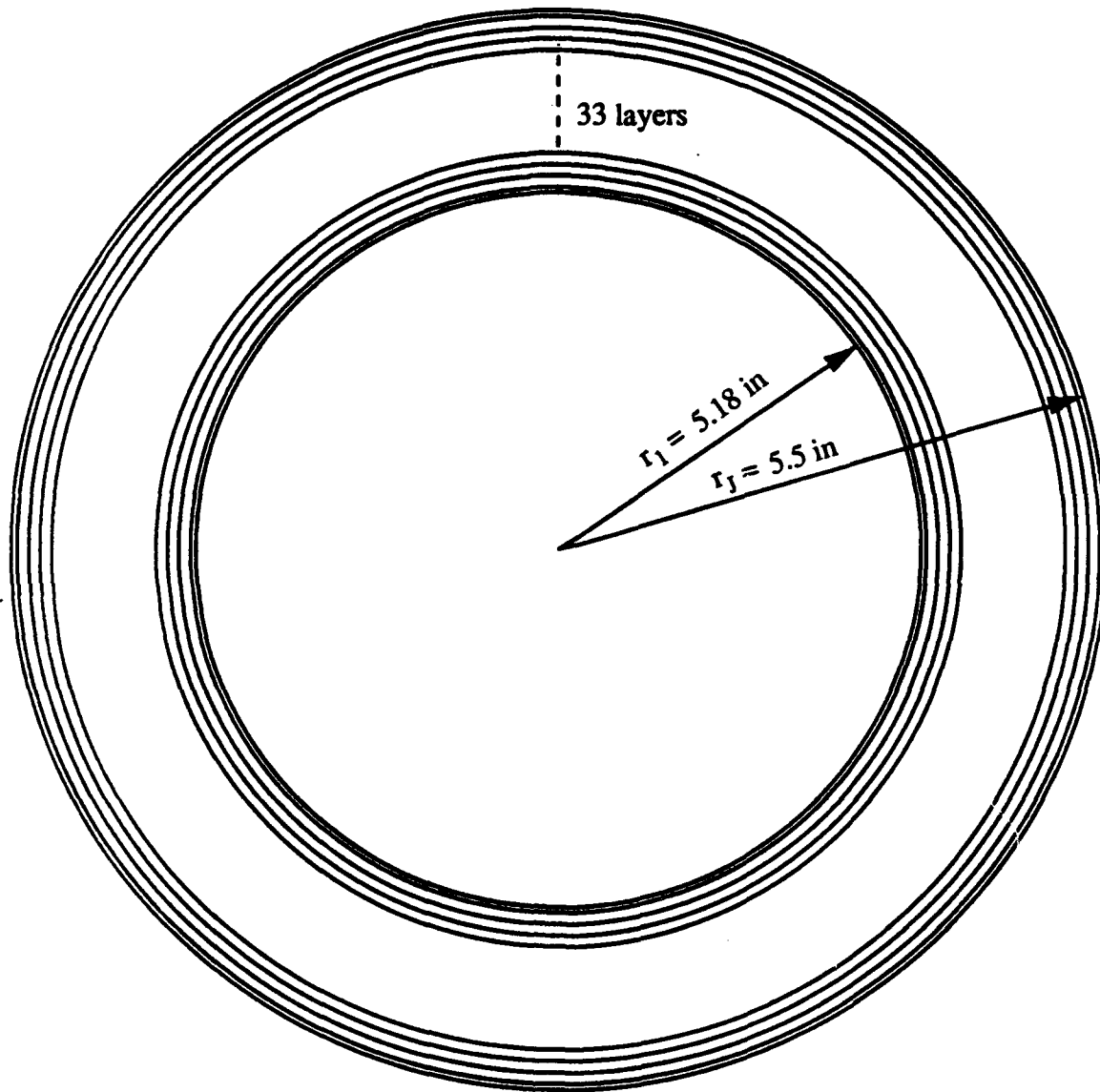


**Figure 11**  
**Configuration of the Cylinder**

Table 3. Geometric, Thermal and Mechanical Parameters for Carbon-Carbon.

Material	Air Core	Layer 1 & 33	Odd Layers	Even Layers
Thickness (in)	$r_1 = 5.18$	0.005	0.01	0.01
Conductivity in r direction (Btu/hr ft°F)	0.0142	12.5	12.5	12.5
Diffusivity in r direction (in <sup>2</sup> /sec)	0.040	0.267	0.267	0.267
Elastic Modulus, (psi)				
$E_r$	---	$0.5 \times 10^6$	$0.5 \times 10^6$	$0.86 \times 10^6$
$E_\theta$	---	$0.5 \times 10^6$	$0.5 \times 10^6$	$3.78 \times 10^6$
$E_z$	---	$0.5 \times 10^6$	$0.5 \times 10^6$	$2.79 \times 10^6$
Poisson's Ratio				
$\nu_{r\theta}$	---	0.33	0.33	0.2
$\nu_{rz}$	---	0.33	0.33	0.4
$\nu_{\theta z}$	---	0.33	0.33	0.05
Coefficient of Thermal Expansion (in./in.°F)				
$\alpha_{r\theta}$	---	$2.30 \times 10^{-6}$	$2.30 \times 10^{-6}$	$2.22 \times 10^{-6}$
$\alpha_{rz}$	---	$2.30 \times 10^{-6}$	$2.30 \times 10^{-6}$	$1.67 \times 10^{-6}$
$\alpha_{\theta z}$	---	$2.30 \times 10^{-6}$	$2.30 \times 10^{-6}$	$1.67 \times 10^{-6}$

larger and the difference between the tangential stresses in the fiber layers and the matrix layers are even smaller.

Assuming that the strengths of the matrix and fiber layers take on those of the carbon-carbon composite (see Section 3) in the parametric study, for the first three cases, the tangential stresses both in the matrix and the fiber layers are smaller than their minimum strength  $R_0$ , hence the reliability of the cylinder is always one. In the last case, the tangential stresses in the fiber layers are much smaller than the minimum fiber strength,  $R_{of}$ , and do not cause failure, but the tangential stresses in the matrix layers in the time range between 0.4 to 2.0 seconds are larger than the minimum matrix strength,  $R_{om}$ . The reliabilities of those matrix layers are almost 0 and the reliability of the cylinder is also almost 0 (Fig. 16).

To improve the reliability of the structure, internal pressure was applied at the innermost surface of the cylinder while subjected to the thermal loading. The internal pressure,  $P_a(t)$ , is molded similarly to the temperature loading:

$$P_a(t) = \begin{cases} 0 & \text{for } t \leq 0 \\ -A\beta t e^{1-\beta t} \text{ psi} & \text{for } t > 0 \end{cases} \quad (64)$$

where the rise time  $t_m$  is chosen as 1 second similarly to that of the thermal loading and A is the maximum value of the internal pressure at  $t = t_m = 1/\beta$ . When  $A = 500$  psi, there is no failure in the matrix layers. The maximum probability of the fiber layers is plotted in Fig. 17. In the time range of 0.0 - 0.5 second and for  $t > 1.5$  seconds, the failure probability of the cyl-



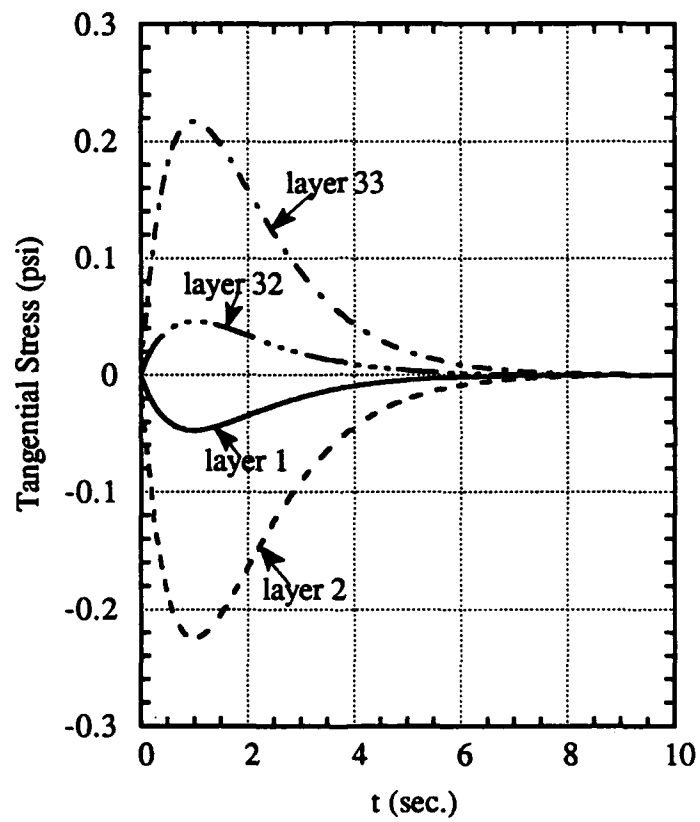


**Figure 12**  
**Tangential Stress in Parameter Study (Case 1)**

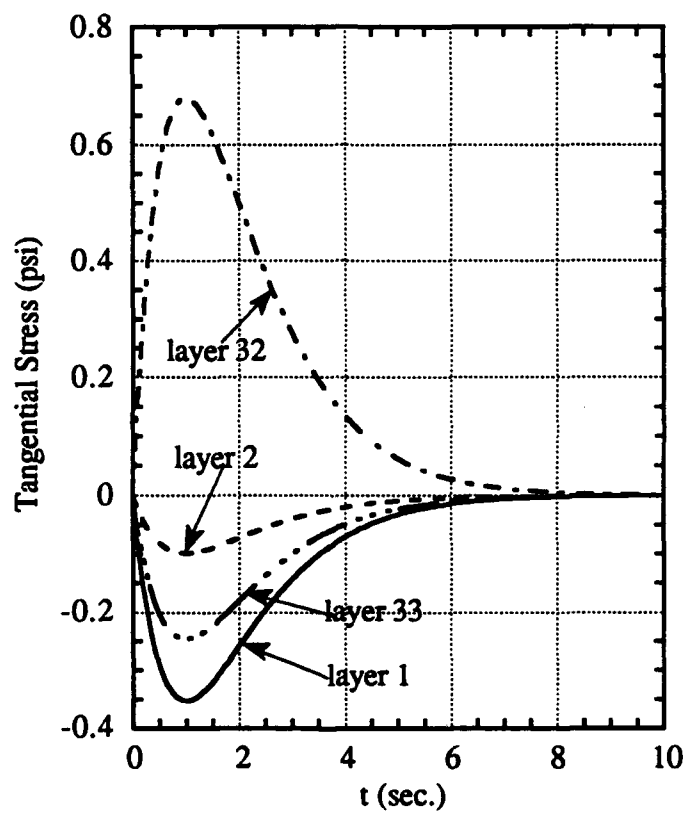


**Figure 13**  
**Tangential Stress in Parameter Study (Case 2)**

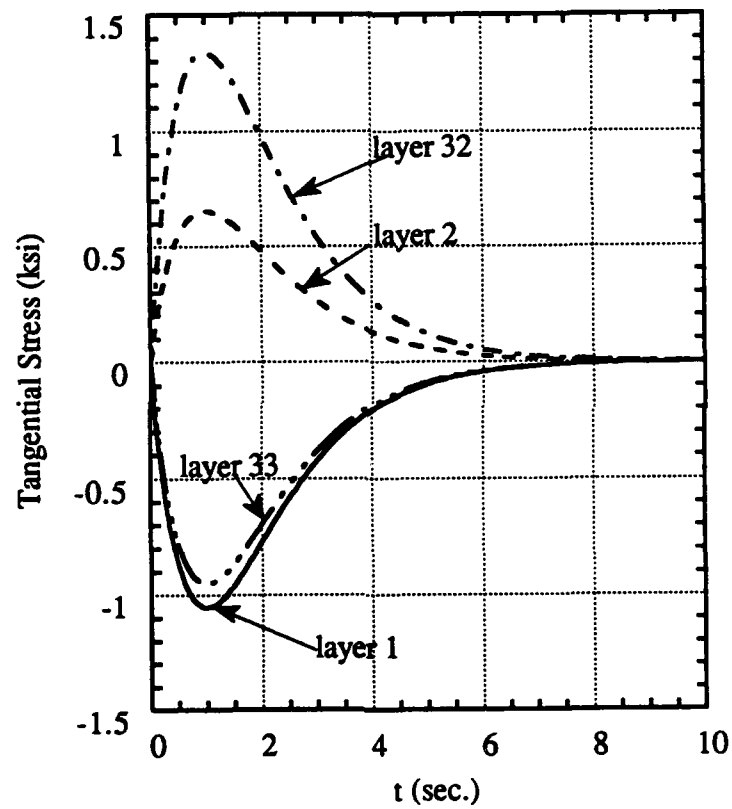


**Figure 14**  
**Tangential Stress in Parameter Study (Case 3)**

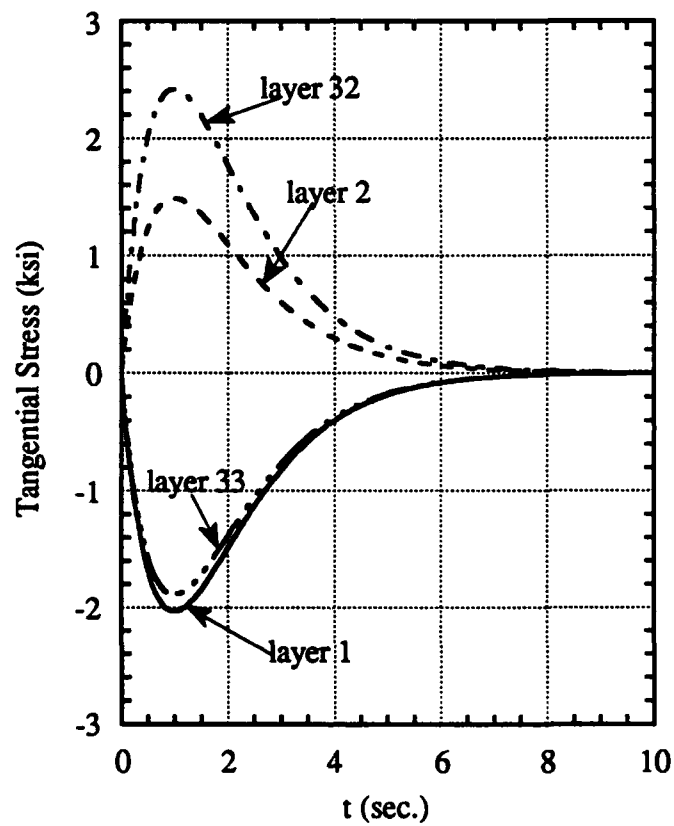


**Figure 15**  
**Tangential Stress in Parameter Study (Case 4)**

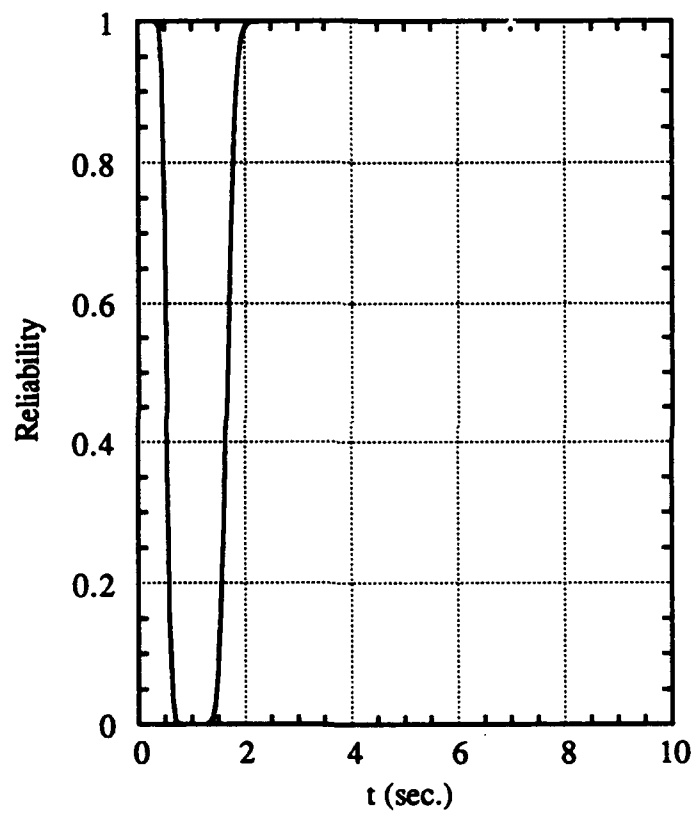


**Figure 16**  
**Reliability of the Cylinder in Parameter Study (Case 4)**

inder is very small and is neglected. The failure probability of the cylinder as a function of time is plotted in Fig. 18.

The above example shows that thermal stress and reliability distributions in a multilayered orthotropic cylinder are sometimes much more complicated than thermal stress and reliability distributions in a multilayered isotropic cylinder. In the above four cases, the materials of the matrix are exactly the same, the elastic moduli are almost the same, and the cylinders are subjected to the same thermal loading, but the first three are safe, the last one fails.

#### The effect of rise time, $t_m$ , on stress distributions

Figs. 19-22 show the maximum tangential stresses at the inner surface of layers 1 and 2, and at the outer surface of layers 32 and 33 of the same cylinder as in the last example above, for different rise times,  $t_m$ , from 1 second to 4 seconds with internal pressure of 400 psi. The rise time,  $t_m$ , has little effect on the maximum tangential stresses at the outer surface of layer 33 when  $t_m$  changes from 1 second to 4 seconds. There are obvious differences on maximum tangential stresses at the rest of the locations mentioned above when rise times are between  $t_m = 1$  second and 2 seconds. The differences are small when  $t_m$  is larger than 2 seconds. This suggests that when rise time,  $t_m$ , is smaller than 1 second, the maximum tangential stress in the cylinder could be very large, and should be calculated very carefully. But when  $t_m$  is larger than 4 seconds, rise time has little effect on the maximum stress.

#### The effect of various internal pressure amplitudes and thermal shock

In this example, the cylinder is subjected to internal thermal shock together with internal pressure,  $P_o(t)$  both with rise times  $t_m = 1$  second. First,  $A = 500$  psi is applied. The tangential stresses plotted in solid lines in Figs. 23-26 are induced by internal pressure alone, while the tangential stresses plotted in dashed lines are induced by both the combined internal thermal shock and pressure. Figs. 27 and 28 show the tangential stresses at different locations in the fiber and matrix layers, while Figs. 29 and 30 show the maximum tangential stress variations through the thickness.

Because the radial stresses in the cylinder are very small, they are neglected in the reliability analysis. It is seen from Fig. 29 that all the tangential stresses in the matrix layers are lower than the minimum strength  $R_{om}$ , and have no contribution to the probability of failure. Failures are due to the tangential stresses in the fiber layers. The maximum tangential stresses in the fiber layers are between 15,893 psi and 16,400 psi, this means that the risk of failure,  $\lambda$ , is very small, and the following equation is quite accurate.

$$P_f = 1 - \prod_{j=1}^n L_j \approx \sum_{j=1}^{n_f} \lambda_j \quad (65)$$

where  $n_f$  is the total number of fiber layers.

The maximum probability failure of the  $j$ th fiber layer,  $P_{fjmax}$ , occurs when the tangential stress of the layer reaches the maximum value. When  $P_{fjmax}$  is small, it is defined as

$$P_{fjmax} = 2\pi \left( \frac{S_{max} - R_0}{R_c - R_0} \right)^m \frac{\bar{r}t}{v_r} \quad (66)$$

where  $\bar{r}$  is the mean radius of the layer and  $t$  is the thickness of the layer while  $P_{fmax}$  is defined as

$$P_{fmax} = \sum_{j=1}^{n_f} P_{fjmax} \quad (67)$$

These maxima occur at different times in different layers and do not coincide. Hence  $P_{fmax}$  represents a worst case and is a conservative estimate.  $P_{fmax}$  is larger than the maximum probability of failure of the cylinder. The failure probabilities,  $P_{fmax}$ , in fiber layers through the thickness are plotted in Fig. 31,  $P_{fmax}$  for the cylinder in this case is  $2.4136 \times 10^{-5}$ . The probability of failure for fiber layers across the wall thickness are shown in Fig. 32 for various rise times.

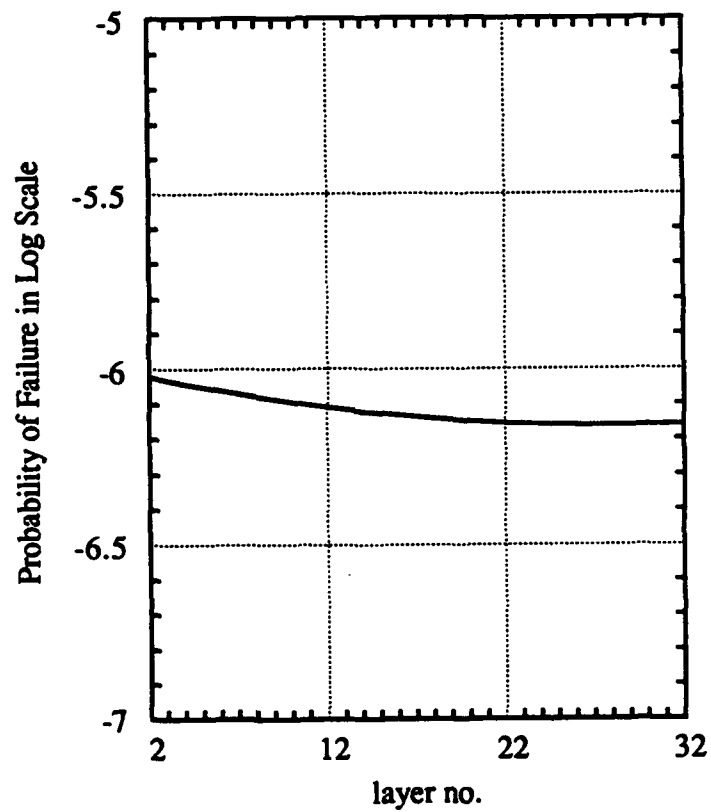


**Figure 17**  
**Probability of Failure of Fiber Layers through the Thickness under Combined Thermal and Pressure Loading**

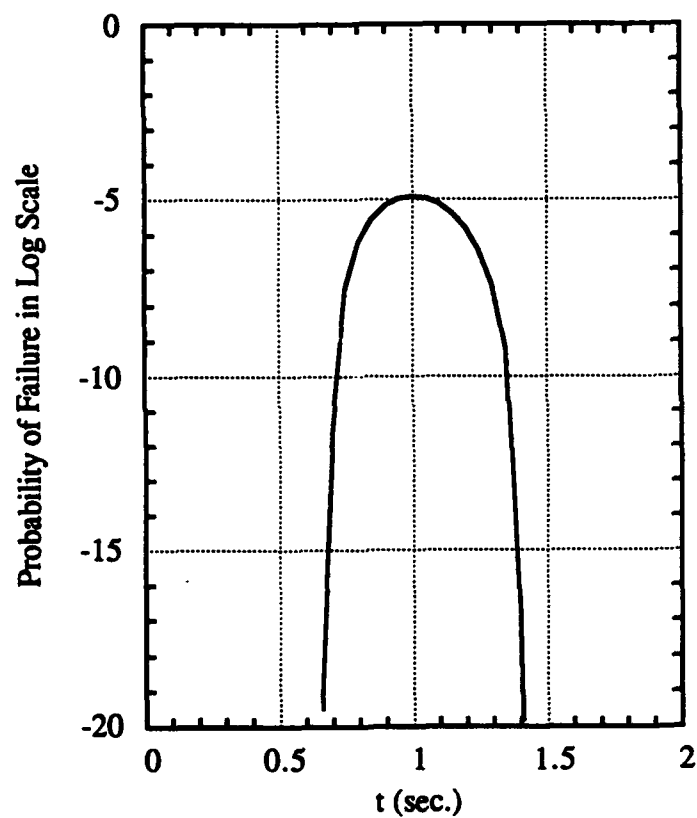


**Figure 18**  
**Probability of Failure of the Cylinder under Combined Thermal and Pressure Loading**



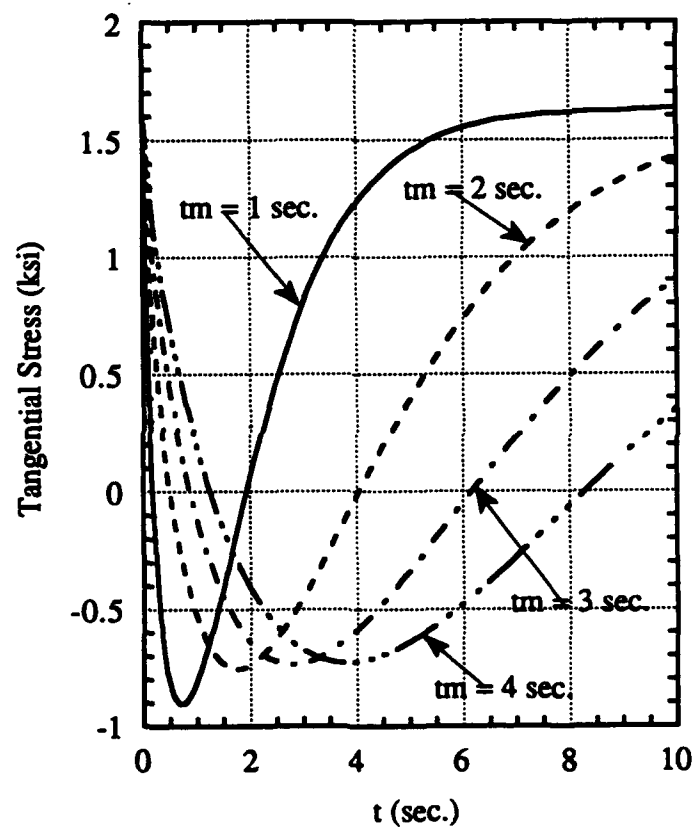


**Figure 19**  
**Tangential Stresses on the Innermost Surface (Matrix Layer); Thermal and Pressure Loading**

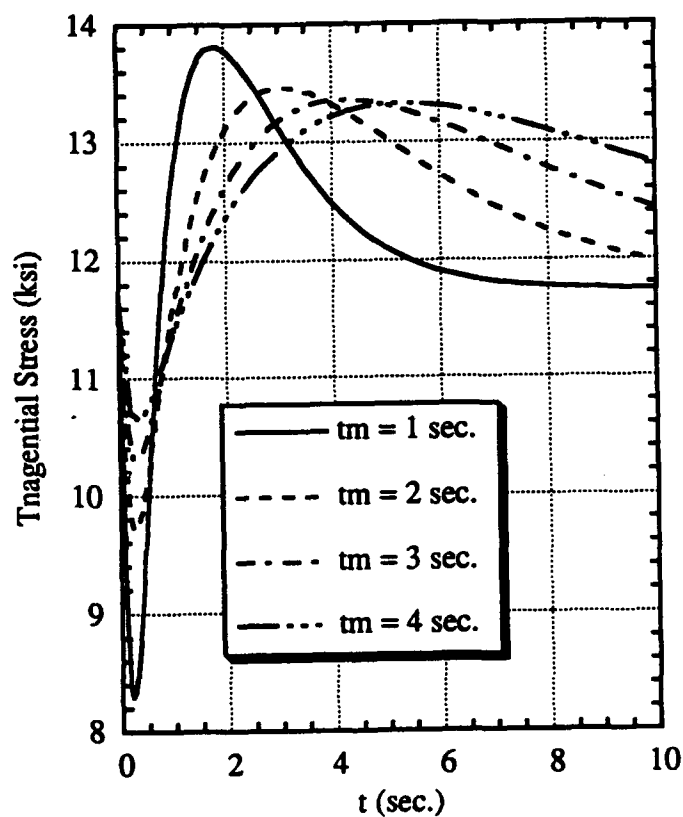


**Figure 20**  
**Tangential Stresses on the Inner Surface of Layer 2 (Fiber Layer); Thermal and Pressure Loading**

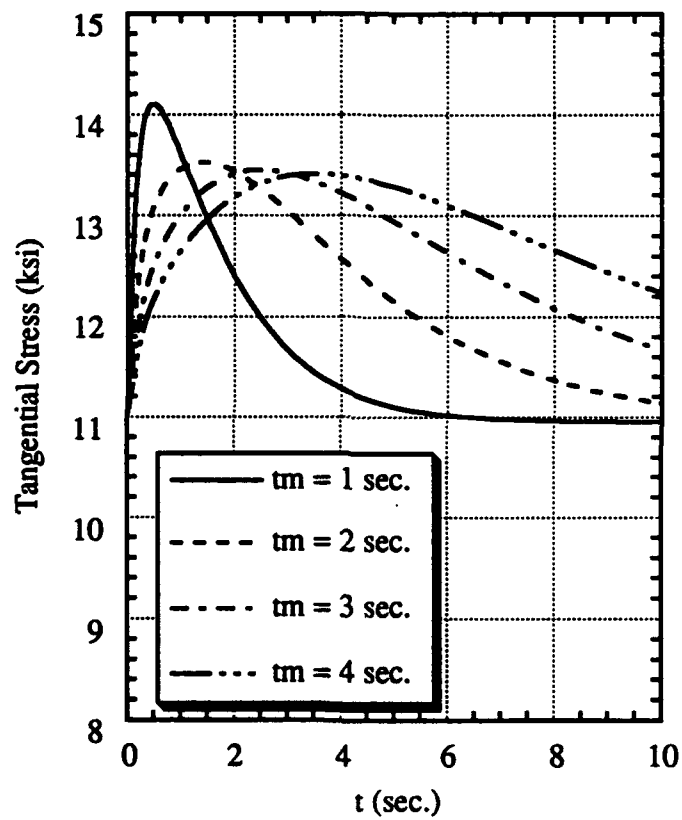


**Figure 21**  
**Tangential Stresses on the Outer Surface of Layer 32 (Fiber Layer); Thermal and Pressure Loading**

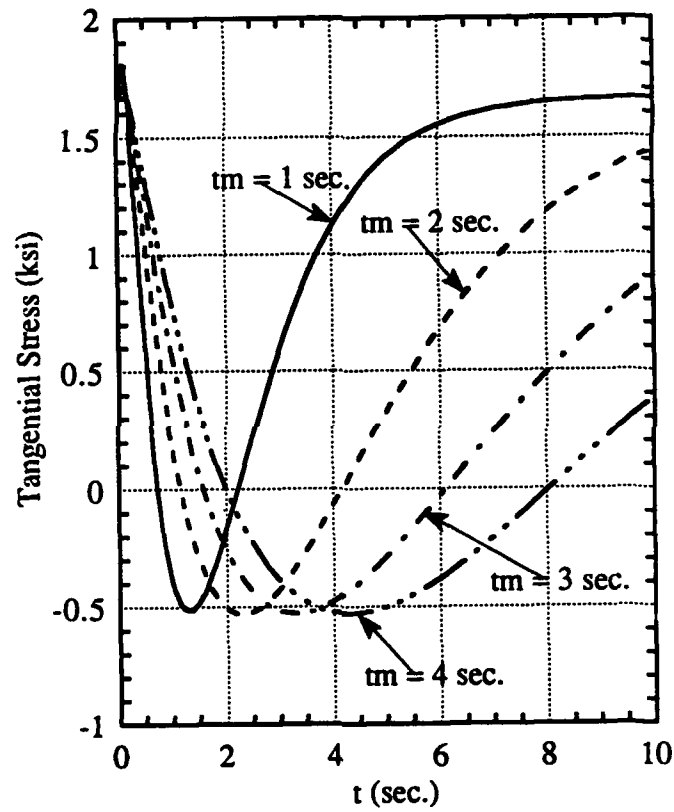


**Figure 22**  
**Tangential Stresses on the Outermost Surface (Matrix Layer); Thermal and Pressure Loading**

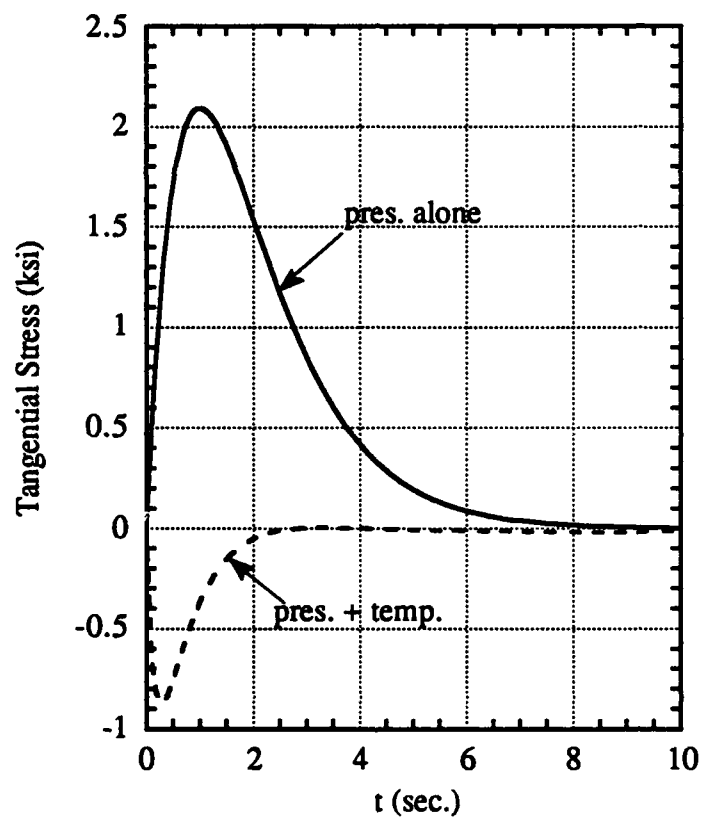


**Figure 23**  
**Tangential Stresses on the Innermost Surface (Matrix Layer) Subjected to Internal Thermal Shock and Internal Pressure**

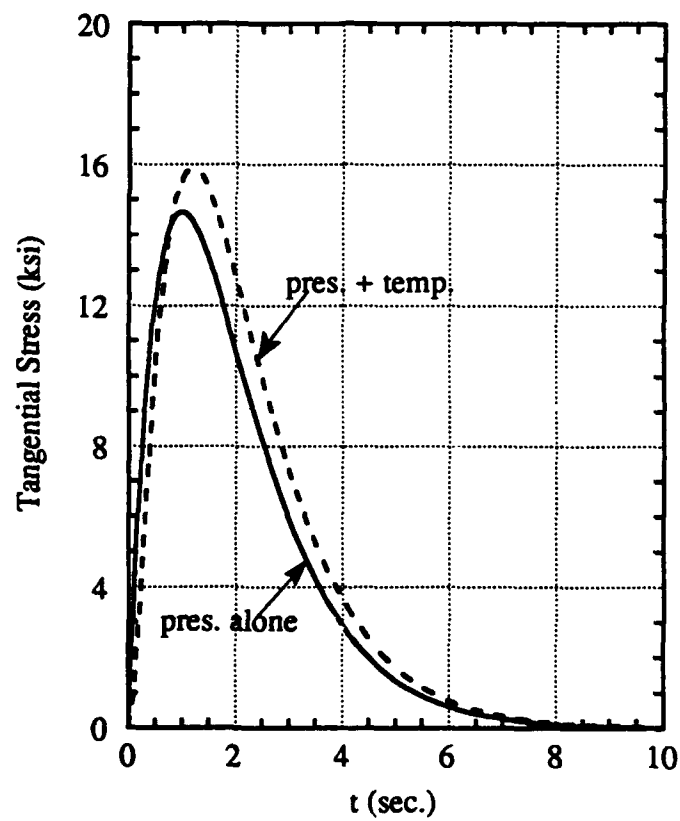


**Figure 24**  
**Tangential Stresses on the Inner Surface of Layer 2 (Fiber Layer) Subjected to Internal Thermal Shock and Internal Pressure**

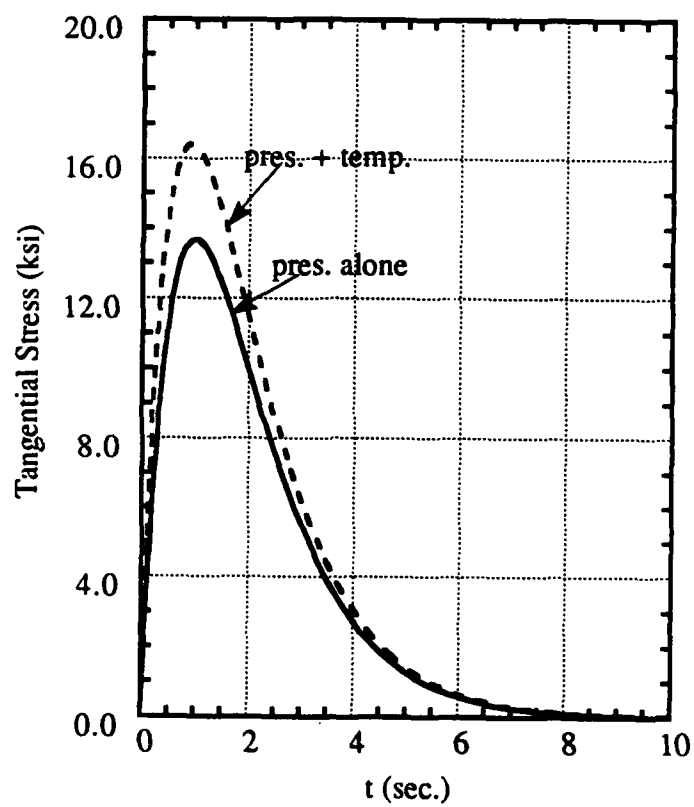


**Figure 25**  
**Tangential Stresses on the Outer Surface of Layer 32 (Fiber Layer) Subjected to Internal Thermal Shock and Internal Pressure**

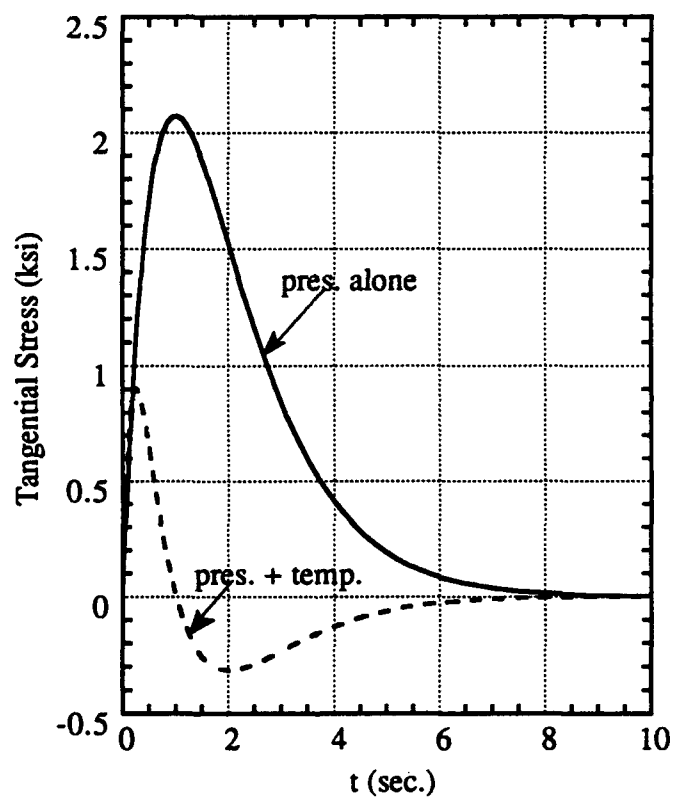


**Figure 26**  
**Tangential Stresses on the Outermost Surface (Matrix Layer) Subjected to Internal Thermal Shock and Internal Pressure**



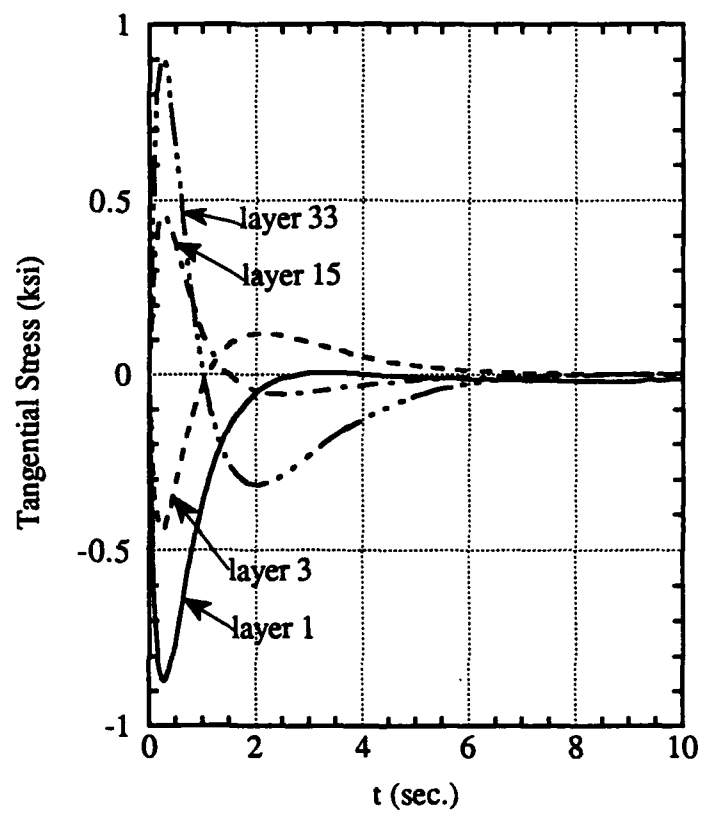


**Figure 27**  
**Tangential Stresses in Different Matrix Layers Subjected to Internal Thermal Shock**

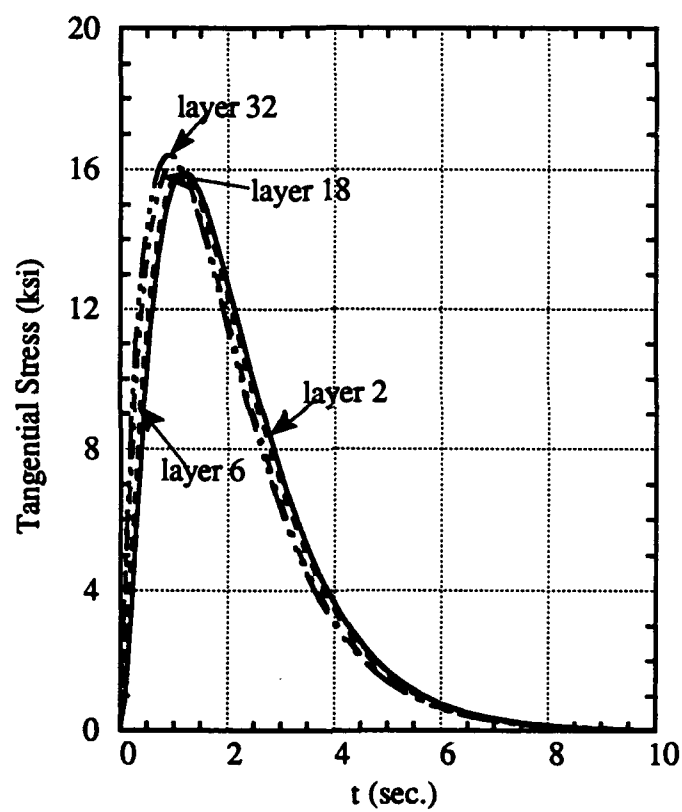


**Figure 28**  
**Tangential Stresses in Different Fiber Layers Subjected to Internal Thermal Shock**

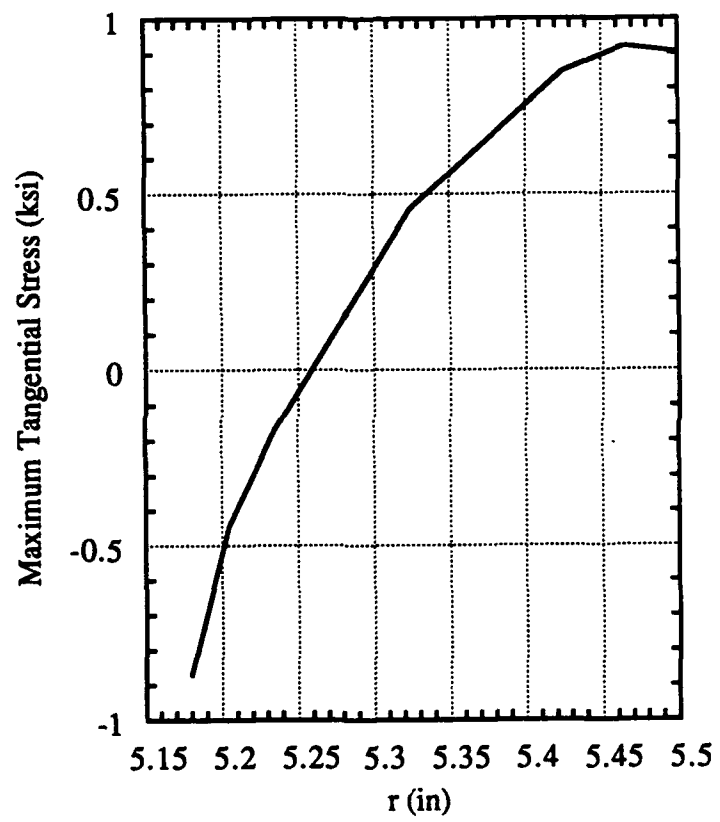


**Figure 29**  
**Maximum Tangential Stresses in Matrix Layers through the Thickness of the Cylinder**

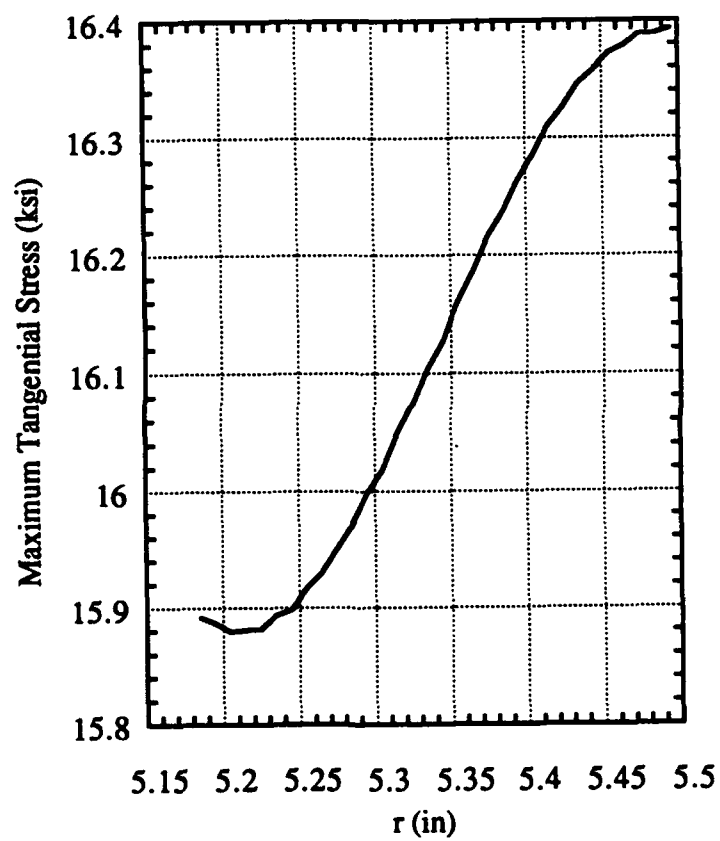


**Figure 30**  
**Maximum Tangential Stresses in Fiber Layers through the Thickness of the Cylinder**

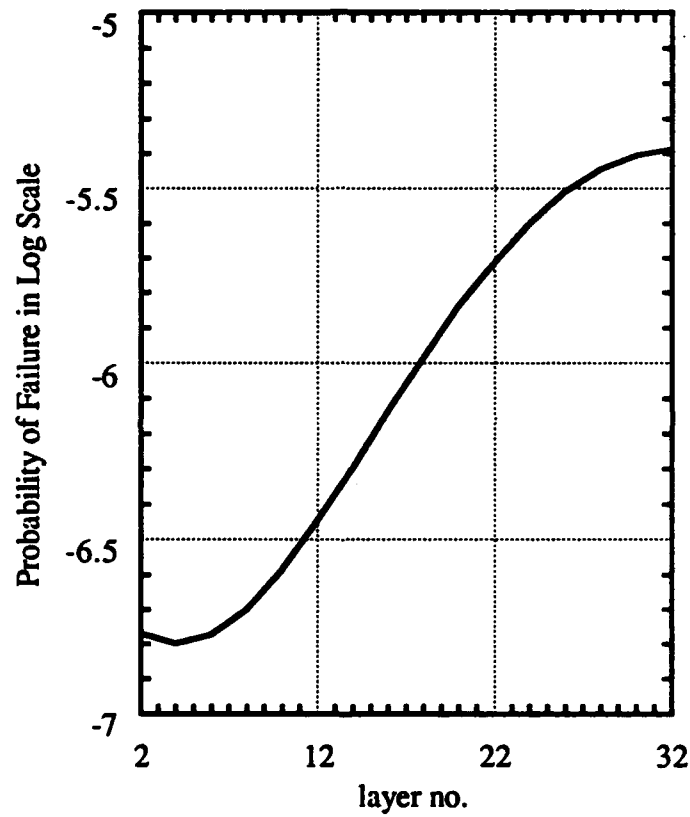


**Figure 31**  
**Maximum Probability of Failure of Fiber Layers through the Thickness of the Cylinder**

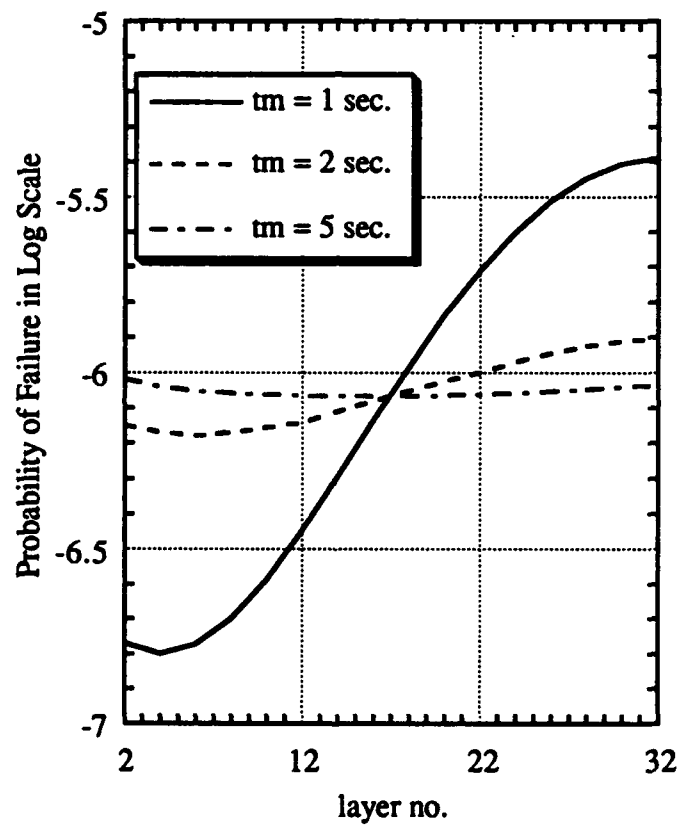


**Figure 32**  
**Maximum Probability of Failure of Fiber Layers through the Thickness of the Cylinder for Different Rise Times**

Now, the maximum internal pressure  $A$  is varied from 0 to 1.0 ksi. The reliabilities of the matrix and fiber layers and of the cylinder under different internal pressures are plotted in Figs 33-35. These Figs show that when  $A$  is between 0.3 - 0.55 ksi, the cylinder is safe, when  $A < 0.3$  ksi, the cylinder fails because the matrix layers fail, and when  $A > 0.55$  ksi, the cylinder fails because the fiber layers fail first.

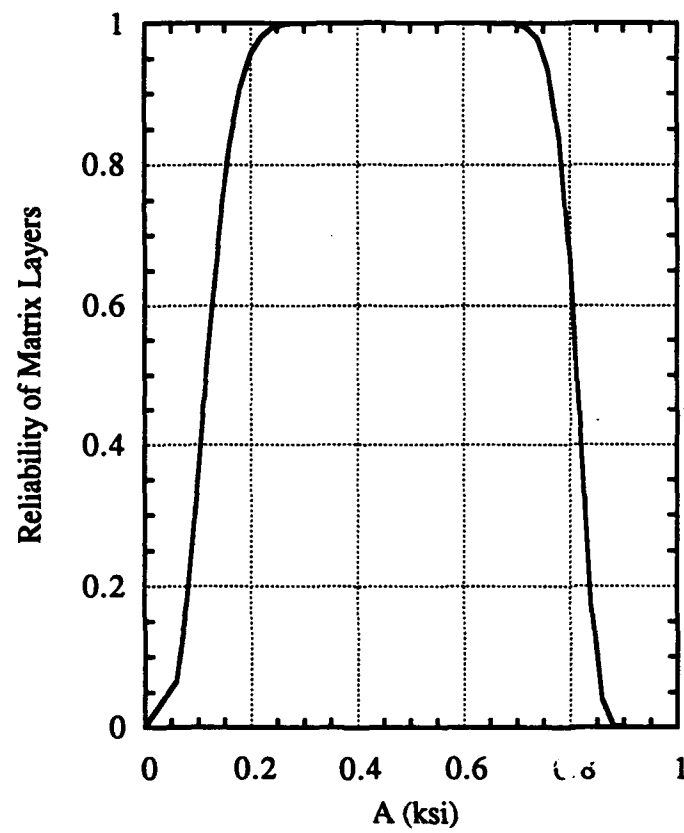


**Figure 33**  
**Reliability of the Matrix Layers Subjected to Thermal Shock and Internal Pressure with Different Amplitudes**



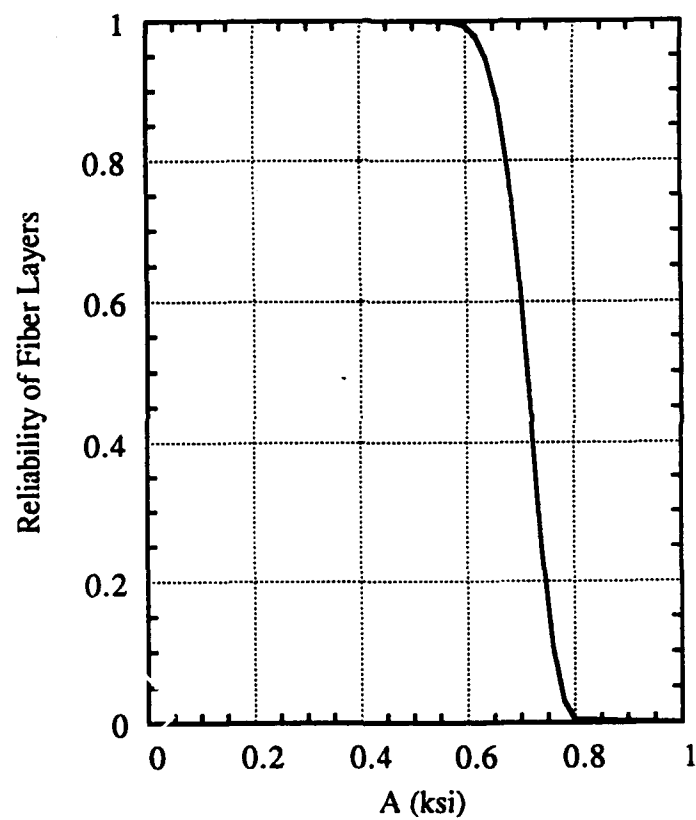


**Figure 34**  
**Reliability of the Fiber Layers Subjected to Thermal Shock and Internal Pressure with Different Amplitudes**

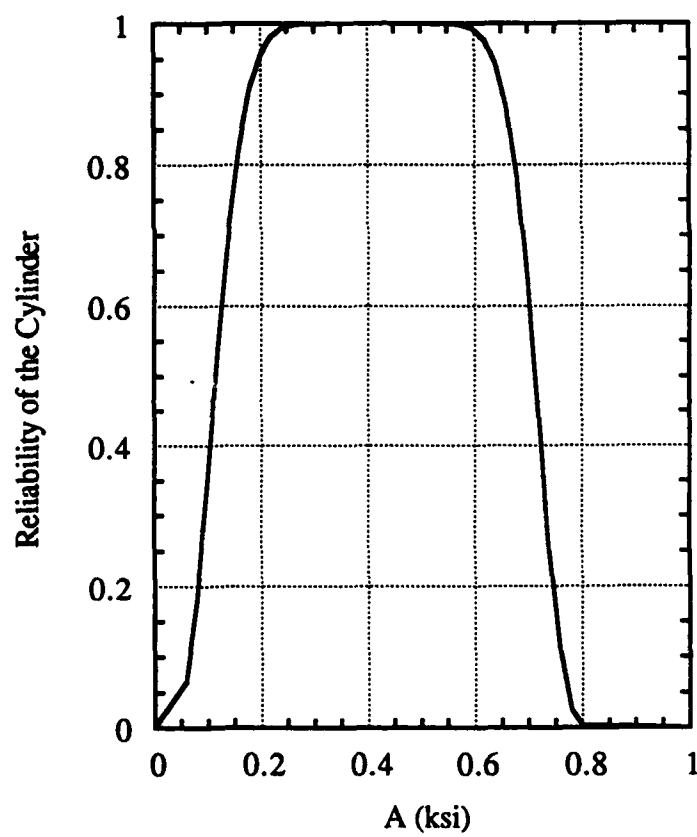


**Figure 35**  
**Reliability of the Cylinder Subjected to Thermal Shock and Internal Pressure with Different Amplitudes**

## SECTION 4. CONCLUSIONS

Thermal shocks have been applied to the internal and external surfaces of a carbon-carbon multilayered hollow cylinder. It has been seen that a large coupling parameter has a significant influence on structural response. Values of the parameter have considerable variations for engineering materials as indicated in Table 2. Because mechanical and thermal properties vary with temperature, the coupling parameter also undergoes thermal changes. Unfortunately information on this temperature dependence is largely unavailable, hence a range of values between zero and 0.5 have been arbitrarily chosen. Coupling affects the results to a lesser extent when the rise time of the input function is longer, that is, when the input temperature varies slowly. In this study, temperature changes rapidly, (rise from room temperature to 3000 °K within only several seconds). For high rates of temperature rise, the coupling effects of thermal and mechanical parameters are important but inertial coupling can be neglected as long as rates are significantly lower than the speed of dilatational waves in the material.

The "weakest link" principle together with the Weibull distribution has been used to calculate the probability of failure for the structure. This method is applicable to brittle materials and is useful for structural components in the present problem. Once the stresses in each element are evaluated, the reliability calculations may be carried out on an element by element basis. The reliability of the structure is then obtained from the product rule.

The illustrations presented indicate that for the particular geometry and thermal shock applied, the structure would fail but the application of an appropriate internal pressure would reduce the induced stresses and the probability of failure as well.

## REFERENCES

1. Heller, R. A., Thangjitham, S., Rantis, T., and Heller, T. G., "Experimental Determination of Mechanical Properties for a Carbon-Carbon Composite", Technical Report, Air Force Phillips Lab., PL-TR-91-3068 4G(1), Edwards AFB., California, April 1991.
2. Heller, R. A., Thangjitham, S., and Yeo, I., "Development of Reliability and Failure Analysis for Carbon-Carbon Structures", Technical Report, Air Force Phillips Lab., PL-TR-91-3068 4G(2), Edwards AFB., California, August 1991.
3. Biot, M. A., "Thermoelasticity and Irreversible Thermodynamics", J. Appl. Physics, vol. 27, March, pp. 240-253, 1956.
4. Dillon, O. W., Jr., "Thermoelasticity When the Material Coupling Parameter Equals Unity", J. Appl. Mechanics, vol. 32, Trans. ASME, vol. 87, pp. 378-382, 1965.
5. Dillon, O. W., Jr., "Coupled Thermoelasticity of a Bar", J. Appl. Mechanics, vol. 34, Trans. ASME, vol. 89, pp. 137-145, 1967.
6. Takeuti, Y. and Tanigawa, Y., "On a New Method for Axisymmetric Coupled Thermoelastic Problems", J. Thermal Stresses, vol. 4, pp. 461-478, 1981.
7. Takeuti, Y. and Tanigawa, Y., "A New Technique for Coupled Plane Thermal Stress Problems", J. Strain Analysis, vol. 17, no. 3, pp. 133-138, 1982.
8. Thangjitham, S., Heller, R. A., and Sing, M. P., "Frequency Response Functions for Thermal Stresses in Multilayered Cylindrical Structures", J. Thermal Stresses, vol. 9, pp. 133-150, 1986.
9. Sing, M. P., Heller, R. A., and Thangjitham, S., "Thermal Stresses in Concentric Cylinders Due to Asymmetric and Time Dependent Temperature Inputs", J. Thermal Stresses, vol. 7, pp. 183-195, 1984.
10. Heller, R. A., Kamat, M. P., Sing, M. P., "Probability of Solid-Propellant Motor Failure Due to Environmental Temperatures", J. Spacecraft and Rockets, vol. 16, no. 3, pp. 140-146, 1979.
11. Kalam, M. A., and Tauchert, T. R., "Stresses in an Orthotropic Elastic Cylinder due to a Plane Temperature Distribution  $T(r, \theta)$ ", J. of Thermal Stresses, Vol. 1, pp. 13-24, 1978.
12. Hyer, M. W., and Cooper, D. E., "Stresses and Deformations in Composite Tubes Due to a Circumferential Temperature Gradient", ASME J. of Applied Mechanics, Vol. 53, pp. 757-764, 1986.
13. Parida, J., and Das, A. K., "Thermal Stresses in a Thin Circular Disc of Orthotropic Material Due to an Instantaneous Point Heat Source", Acta Mechanica, Vol. 13, pp. 205-214, 1972.

14. Tauchert, T. R., "Thermal Shock of Orthotropic Rectangular Plates, J. of Thermal Stresses", Vol. 12, pp. 241-258, 1989.
15. Tanigawa, Y., Murakami, H., and Ootao, Y., "Transient Thermal Stress Analysis of a Laminated Composite Beam", J. of Thermal Stresses, Vol. 12 pp. 25-39, 1989.
16. Wang, Y. R., and Chou, T. W., "Three-Dimensional Transient Interlaminar Thermal Stresses in Angle-Ply Composites", ASME J. of Applied Mechanics, Vol. 56, pp. 601-608, 1989.
17. Boley, A. B. and Weiner, J. H., "Theory of Thermal Stresses", Wiley, New York, 1960.
18. Wang, X., Thangjitham, S., and Heller, R. A., "Response of a Multilayered Cylinder to Thermal Shock", J. Thermal Stresses, Vol. 14, pp. 47-64, 1991
19. R. A. Heller, S. Thangjitham, and X. Wang, "Structural Reliability of Reactor Fuel Rods after Emergency Cooling", Applied Mechanics Review, 1991,
20. Abramowitz, M. and Stegun, I. A., eds., "Handbook of Mathematical Functions", Dover, New York, 1972.
21. Weibull, W., "Investigations into Strength Properties of Brittle Materials", Proceedings of the Royal Swedish Institute for Engineering Research, No. 149, pp. 1-27, 1938.
22. Stanley, P., Sivill, A. P., and Fessler, H., "The Application and Confirmation of a Predictive Technique for the Fracture of Brittle Components", Paper No. 22, Proc. Fifth Intl. Conf. on Exper. Stress Anal., Udine, Italy, 1974.
23. Margetson, J., "A Statistical Theory of Brittle Failure for an Anisotropic Structure Subjected to a Multiaxial Stress State", Am. Inst. of Aeronautics and Astronautics, 12th Propulsion Conf. Paper No. 76-632, Palo Alto, CA, July 26-29, 1976.
24. Franklin, Philip, "An Introduction to Fourier Methods and the Laplace Transformation", Dover, New York, 1958.
25. Crandall, S. H. and Mark, W. D. "Random Vibrations in Mechanical Systems", Academic Press, New York, 1963.
26. Bolz, Ray E., Tuve, George L., "Handbook of Tables for Applied Engineering Science", the Chemical Rubber Co., 1970.
27. Hercules, "Advanced Composites", Technical Data, Bulletin ACM-7, 9A.
28. Christos C. Chamis, "Simplified Composite Micromechanics for Hygral Thermal and Mechanical Properties", 38th Annual Conference, Reinforced Plastics/ Composites Institute, Session 21-C, pp. 1-9, 1983
29. Heller, R. A., Schmidt, A., and Denninghoff, R., "The Weakest Link Concept after Proof Testing", in Probabilistic Methods in the Mechanics of Solids and Structures, IUTAM Symposium Stockholm, 1984, Springer, Berlin 1985.